

**THE INFLUENCE OF CONNECTED HETEROGENEITY IN
HYDRAULIC CONDUCTIVITY ON GROUNDWATER FLOW AND
SALINITY DISTRIBUTIONS IN A COASTAL VOLCANIC AQUIFER**

by

Pieter Kreyns

A thesis submitted to the Faculty of the University of Delaware in partial fulfillment of the requirements for the degree of Master of Science in Geology

Fall 2019

© 2019 Pieter Kreyns
All Rights Reserved

**THE INFLUENCE OF CONNECTED HETEROGENEITY IN
HYDRAULIC CONDUCTIVITY ON GROUNDWATER FLOW AND
SALINITY DISTRIBUTIONS IN A COASTAL VOLCANIC AQUIFER**

by

Pieter Kreyns

Approved: _____
Holly Michael, Ph.D.
Professor in charge of thesis on behalf of the Advisory Committee

Approved: _____
John A. Madsen, Ph.D.
Interim Chair of the Department of Earth Sciences

Approved: _____
Estella Atekwana, Ph.D.
Dean of the College of Earth, Ocean, and Environment

Approved: _____
Douglas J. Doren, Ph.D.
Interim Vice Provost for Graduate and Professional Education and
Dean of the Graduate College

TABLE OF CONTENTS

LIST OF TABLES	iv
LIST OF FIGURES	v
ABSTRACT	viii

Chapter

1 INTRODUCTION	1
2 METHODS	5
3 RESULTS	13
4 DISCUSSION	24
5 CONCLUSION	27
REFERENCES	29

Appendix

A TOP-DOWN SALINITY DISTRIBUTIONS FOR EVERY REALIZATION	38
B TOP-DOWN SGD AND SGR DISTRIBUTIONS FOR EVERY REALIZATION	42
C TABLE OF EFFECTIVE HYDRAULIC CONDUCTIVITIES, RATIOS, AND LANDWARD SEAWATER EXTENT FOR EACH HOMOGENEOUS REALIZATION	46
D SALINITY AND HYDRAULIC CONDUCTIVITY CROSS-SECTIONS FOR ALL REALIZATIONS	47

LIST OF TABLES

Table 1	Hydraulic conductivity values, Garcia et al. (2007) percentages, and approximate percentage of the total domain for each of the six facies in the geologic model. Where applicable, sources are given for each K value.	7
Table 2	Parameter values used in variogram models for each geologic facies. Note that the exponential variogram model, $\gamma(h) = C(1 - e^{-\frac{h}{a_h}})$, was adopted in geostatistical simulations, where C is sill, a_h is range, and h is the distance between each pair of points.	9

LIST OF FIGURES

Figure 1	SEAWAT model domain.	11
Figure 2	Normalized hydraulic conductivity fields (b, d, f) and salinity distributions (a, c, e) for selected conduit (a, b), SIS (c, d) and homogeneous (e, f) realizations.	14
Figure 3	Average x-location (in meters) of centers of mass of brackish ($1 < \text{ppt} < 34$) body (top panel), onshore extent of saline water (middle panel), and offshore extent of freshwater (bottom panel) for each homogeneous and conduit model realization. Error bars in the top panel represent range of body extents across all cross-sections in conduit cases. Error bars for homogeneous cases were minimal.	16
Figure 4	Average mixing zone volume (a) and center of mass x-location (b) across all realizations. Red lines indicate the median data value. Top and bottom of the rectangles represent the 25 th and 75 th percentile of the dataset, and error bars indicate maximum and minimum volume and extent, respectively. Red crosses indicate potential outlier data.	17
Figure 5	SGD (left) and SGR (right) values for conduit (top), homogeneous (center), and SIS (bottom) realizations. Shoreline is at the leftmost boundary of plots.	19
Figure 6	Flux variance in the transverse alongshore direction for conduit (top), homogeneous (center), and SIS (bottom) models for three example realizations.	20
Figure 7	Comparison of average fresh (a) and saline (b) discharge rates across model domains. Error bars indicate maximum and minimum values across seven realizations.	21
Figure 8	Comparison of the saline SGD/fresh SGD ratio between model simulations.	22
Figure 9	Histograms of log discharge for all conduit, SIS, and homogeneous cases.	23
Figure A1.	Salinity distributions for Realization 1 (ppt).	38
Figure A2.	Salinity distributions for Realization 2 (ppt).	38
Figure A3.	Salinity distributions for Realization 3 (ppt).	39

Figure A4. Salinity distributions for Realization 4 (ppt).....	39
Figure A5. Salinity distributions for Realization 5 (ppt).....	40
Figure A6. Salinity distributions for Realization 6 (ppt).....	40
Figure A7. Salinity distributions for Realization 7 (ppt).....	41
Figure B1. SGD and SGR distributions for Realization 1.....	42
Figure B2. SGD and SGR distributions for Realization 2.....	42
Figure B3. SGD and SGR distributions for Realization 3.....	43
Figure B4. SGD and SGR distributions for Realization 4.....	43
Figure B5. SGD and SGR distributions for Realization 5.....	44
Figure B6. SGD and SGR distributions for Realization 6.....	44
Figure B7. SGD and SGR distributions for Realization 7.....	45
Figure D1. Salinity (left) and hydraulic conductivity (right) cross-sections for conduit (top), SIS (middle), and homogeneous (bottom) cases of Realization 1.....	47
Figure D2. Salinity (left) and hydraulic conductivity (right) cross-sections for conduit (top), SIS (middle), and homogeneous (bottom) cases of Realization 2.....	48
Figure D3. Salinity (left) and hydraulic conductivity (right) cross-sections for conduit (top), SIS (middle), and homogeneous (bottom) cases of Realization 3.....	49
Figure D4. Salinity (left) and hydraulic conductivity (right) cross-sections for conduit (top), SIS (middle), and homogeneous (bottom) cases of Realization 4.....	50
Figure D5. Salinity (left) and hydraulic conductivity (right) cross-sections for conduit (top), SIS (middle), and homogeneous (bottom) cases of Realization 5.....	51
Figure D6. Salinity (left) and hydraulic conductivity (right) cross-sections for conduit (top), SIS (middle), and homogeneous (bottom) cases of Realization 6.....	52

Figure D7. Salinity (left) and hydraulic conductivity (right) cross-sections for conduit (top), SIS (middle), and homogeneous (bottom) cases of Realization 7..... 53

ABSTRACT

The mixing zone of coastal aquifers, the region where fresh terrestrial groundwater interacts with saltwater, plays a critical role in solute flux to and from the ocean. Knowledge of the geologic structure and pathways of groundwater input to this zone is crucial for predicting effects on coastal ecosystems and ocean health. These same pathways may also allow for seawater intrusion, making knowledge of their influence a priority for both inland and offshore water chemistry. Groundwater and associated solutes can be preferentially channeled through highly connected geologic structures, such as lava tube systems in the volcanic aquifers of Hawaii. To better understand how the complex geology of volcanic systems affects water fluxes between land and sea in coastal regions, we created a geologic model composed of high-permeability lava tubes surrounded by lower-permeability lava and ash. The model was constructed with a surface-based geostatistical method using geometrical parameters extracted from process-based simulations. We investigated the effects of this hydraulic heterogeneity on the rate and spatial distribution of submarine groundwater discharge and subsurface salinity distributions with simulations of variable-density groundwater flow and salt transport. We also compared the connected hydraulically heterogeneous simulations to homogeneous simulations with upscaled equivalent permeability as well as simulations with a different heterogeneous geometry. We found that simulations with connected heterogeneity have larger mixing zones, higher volumes of recirculated seawater, and contained farther offshore freshwater and less onshore seawater. The results have implications for coastal water resource management and provide a better understanding of geologic controls on solute flux between land and sea in volcanic systems.

Chapter 1

INTRODUCTION

Coastal aquifers are a primary source of freshwater for many populations around the globe. Despite their prevalence as a water resource, however, they are particularly vulnerable to problems that include contamination from both onshore and offshore pollutants (Böhlke and Denver, 1995; DeSimone and Howes, 1996; Kroeger et al., 2007; Almasri, 2008) and aquifer salinization (Kim et al., 2003; Park et al., 2005; Barlow and Reichard, 2010). Nearshore surface waters also suffer from pollution derived from discharge of groundwater and surface water, resulting in problems such as eutrophication (Lapointe and Matzie, 1996; Paerl, 2003; Hwang et al., 2005; Paytan et al., 2006). To protect coastal water resources for both humans and ecosystems, we must understand both saltwater intrusion (SWI; Bear et al., 1999), the movement of saline water into fresh aquifers, and submarine groundwater discharge (SGD), the flow of groundwater into coastal water bodies.

Understanding salinity distributions in coastal aquifers as well as past and future landward movement of salt are important for managing fresh groundwater resources. SWI can happen naturally (e.g. as a result of sea-level rise) or artificially (e.g. induced through pumping). Many studies have mapped or simulated SWI in coastal regions (e.g., Segol and Pinder, 1976; Huyakorn et al., 1987; Giambastiani et al., 2007; Barlow and Reichard, 2010). There have also been many field campaigns to understand the landward extent of SWI and attempt to mitigate intrusion (e.g., Melloul

and Goldenberg, 1997; Mulrennan and Woodroffe, 1998; Cruz and Silva, 2000). Much of the modeling work to date on coastal groundwater salinity distributions and seawater intrusion has focused on simplified homogeneous systems, using simple analytical solutions (Bussman and Suess, 1998; Robinson et al., 2006) or numerical models with simplified geology (Li et al., 1999; Uchiyama et al., 2000).

An important factor in the understanding of salinity distributions and SWI is geologic and hydraulic heterogeneity (Barlow and Reichard, 2010; Werner et al., 2013). The nature of the geologic setting creates unique patterns of solute transport (Hu et al., 2009). Much work has been done in the field of contaminant transport related to fractured systems (Tang et al., 1981; Sudicky and Frind, 1982; Sebben et al., 2015), low-permeability barriers (Sebben and Werner, 2016), and statistically-generated heterogeneity (Cushman et al., 1995; Li et al., 2009; Sebben et al., 2012;). Connected features such as paleovalleys, karstic fractures, and lava tubes have been studied in terrestrial systems and shown to be critical to solute transport due to the formation of preferential groundwater flow patterns (Kung, 1990; Webb and Anderson, 1996; Hendrickx and Flury, 2001). In coastal systems, it has been found that low-permeability barriers (e.g. dikes) that intersect an aquifer can reduce the effect of SWI (Comte et al., 2017) whereas high-permeability channels (e.g. lava tubes or paleovalleys) can create preferential flowpaths for SWI (Goebel et al., 2017; Mulligan et al., 2006; Russoniello et al., 2013).

SGD to is also a global phenomenon (Moore, 1999; Burnett et al., 2003) and can be comprised of fresh, terrestrial water as well as saline water recirculated from the ocean (Moore, 2010). SGD can contribute large fluxes of solutes (e.g. nutrients, metals, carbon, and radioactive tracers; Moore, 1996; Moore et al., 2002; Burnett et

al., 2007; Slomp and Van Cappellen, 2004; Sawyer et al., 2016; Bishop et al., 2017), leading to increased primary production (Paytan et al., 2006; Street et al., 2008) and algal blooms (Paerl, 1997; Kim et al., 2003; Hwang et al., 2005; Fabricius, 2005; Lee and Kim, 2007; Lee et al., 2009).

In heterogeneous systems, the spatial patterns of discharge can be complex, which complicates measurement and modeling of the process (Michael et al., 2003; Taniguchi et al., 2003; Schlüter et al., 2004; Burnett et al., 2006). Geologic heterogeneity can enhance SWI (Pool et al., 2015), increase seawater recirculation (Kerrou and Renard, 2010; Michael et al., 2013), increasing total SGD (Stieglitz et al., 2008; Kalbus et al., 2009). More generally, heterogeneity increases the uncertainty of the model results (Schornberg et al., 2010). Studies have also shown that the geometry of heterogeneity is a critical factor in both salinity distributions and SGD (Cherkauer and Nader, 1989; Mulligan et al., 2006).

One such real-world system with unique spatial heterogeneity are volcanic systems. These aquifers, present in Hawaii and other areas, are highly heterogeneous and contain numerous high-conductivity conduits (lava tubes) in an otherwise low-conductivity matrix (basalt) that can influence SGD and SWI. Indeed, field investigations of SGD in Hawaii have shown evidence of point discharge of groundwater into offshore waters (Johnson et al., 2008; Street et al., 2008; Peterson et al., 2009), a feature that will not typically exist without unique geometry in a coastal environment. These observations of discharge are likely due to lava tubes, well documented features in Hawaii (Greeley, 1971; Fornari, 1986; Koeppen et al., 2013). Lava tubes could play a crucial role in aquifer dynamics due to their high hydraulic conductivity (K). However, current models of the coasts of Hawaii and other similar

islands assume a homogeneous (or near-homogeneous) hydraulic conductivity field system for ease of computation (Souza and Voss, 1987; Oki, 1999; Gingerich and Voss, 2005). As already discussed, however, the influence of heterogeneity, and specifically unique patterns of heterogeneity, cannot be understated.

To date, the influence of continuous, high-K conduit features on rates and patterns of SGD and salinity distributions in the subsurface has not been characterized quantitatively. Here we use numerical modeling to compare heterogeneous systems containing conduits to heterogeneous systems with less-continuous features and equivalent homogeneous aquifers. We developed numerical models that represent a portion of the coastline of the Big Island of Hawaii. This area was chosen due to the fact that previous studies have already observed the effects of unique heterogeneity and provided some results for comparison to our own. In general, however, our hypothetical coastline represents any potential system with high-K conduits running through an otherwise low-K matrix. Within this, we simulated variable-density groundwater flow and salt transport to examine geologic influence on salinity distributions and rates and patterns of both fresh and saline SGD.

Chapter 2

METHODS

Lava Flow Model

A three-dimensional hybrid deterministic and geostatistical numerical model of volcanic depositions from multiple eruption events (Koneshloo et al., 2018) was modified to simulate the volcanic deposits of Hualalai volcano on the western side of the Big Island of Hawaii. This volcano was chosen due to its being responsible for lava flows in the region of past SGD studies on the Big Island. Because three-dimensional simulation of an entire volcano from vent to the shoreline is time-consuming and only a small portion is needed for the study area, lava flows were generated randomly along a row of vents 20 kilometers (km) inland from the shoreline (10km closer than the actual vent). The initial digital elevation model (DEM) from Koneshloo et al. (2018) was a 8km x 1km grid with 10m x 10m cells for a total grid of 800 x 100 cells with a constant slope of 0.0625. Elevation ranged from 500m at the top to 0m at the bottom in accordance with the original model setup. Lava flows were constrained by no-flow boundaries along the landward and shore-perpendicular edges of the model domain. Lava flows were simulated from vents at the highest point of the DEM that consisted of six volcanic rock types: a'a, clinker, transitional lava, pahoehoe, ash, and lava tubes. Individual lava flows started flowing from a single cell vent and were allowed to flow across the DEM and were composed of a 90m wide, >3m deep channel of solid aa in the majority of simulated lava flows. An interior, 1m wide, channel was replaced by lava tube conduits in 8% of flows and by transitional

lava in 17.5% of flows. Pahoehoe was simulated as an inflated field extending from the end of lava flows (Hon et al., 1994). Ash was simulated as a thin, nearly-uniform deposit across the entire domain, with decreasing thickness with distance from the vent, occurring for 1% of eruption events. Two meters of clinker were deposited on top of each a'a deposit (Macdonald, 1972). Proportions of the six facies are given in Table 1. Facies probabilities and some dimensions (e.g., size of inflated pahoehoe fields) were chosen to approximate proportions observed in a core through Mauna Loa and Mauna Kea deposits ~40km from a vent (Garcia et al., 2007), but with higher a'a and lower pahoehoe proportions to represent a Hualalai-type system at a distance of ~12km from a vent (Rowland and Walker, 1990; Wentworth and Macdonald, 1953). The distance of 12km was chosen to represent the distance from the western coastline to the main vent complex of Hualalai. To achieve this, pahoehoe fields were extended 300m out from the end of lava tubes instead of kilometers as can sometimes be seen in the field, and thickness was varied between 1m and 3m (Hon et al., 1994). Fifteen thousand flow events were simulated to generate large, three-dimensional heterogeneous deposits. This process was completed seven times to generate seven unique heterogeneous fields. These seven unique realizations were simulated in order to create hydraulic conductivity fields for multiple, statistically independent volcanic aquifer models.

Table 1 Hydraulic conductivity values, Garcia et al. (2007) percentages, and approximate percentage of the total domain for each of the six facies in the geologic model. Where applicable, sources are given for each K value.

Facies	Simulated Facies Percentages (Avg.±St. Dev)	Garcia et al. Section Percentage	Hydraulic Conductivity (m/s)	Hydraulic Conductivity Source
A'a	74.07±3.56	44.7	10 ⁻⁷	Hunt, Jr. et al., 1988
Transitional	3.40±0.85	9.5	10 ⁻⁶	N/A
Pahoehoe	10.17±3.41	44.8	10 ⁻⁵	Anderson et al., 1999
Clinker	5.68±0.56	N/A	10 ⁻³	Miller et al., 2000
Basaltic Ash	0.21±0.05	0.5	10 ⁻⁹	Ducci, 2010
Lava Tube	6.47±2.08	N/A	10 ⁻¹	N/A

Groundwater Flow Model

Due to the size of the original numerical model, a smaller section of the model, representing the saturated portion of a nearshore volcanic aquifer, was selected as the domain for simulating nearshore groundwater flow and salt transport processes at a distance of approximately 12km from the Hualalai vent. Model discretization was set at 100 x 30 x 100 cells, the same as the geologic model. The size of the domain was 1000m in the across shore direction (shoreline was located at 500m) and 300m in the alongshore direction. The vertical depth of the domain was 100m for the onshore part up to the shoreline, and gradually decreased to 10m at the offshore boundary (Figure 1). Since the vertical cell count does not change, the vertical length of each offshore cells ranges from 1m to 0.1m depending on distance from the shoreline. The size of each cell, therefore, was 10m x 10m x 1(0.1)m. The onshore slope is 0, due to the

near-horizontal water table in the nearshore environment of western Hawaii, it is not necessary to simulate the thick unsaturated zone above sea level. The resulting offshore slope of 0.18 is consistent with nearshore bathymetry in that area (NCEI, 2018).

Postprocessing of the numerical model was necessary to connect cells representative of lava tubes to represent continuous high-K structures for the flow and transport simulations. Whereas the numerical model considered edge-connected cells to be continuous, groundwater modeling software requires continuous cells to be face-connected. As such, individual cells belonging to the same lava tube flow were isolated, and the interstitial cells were converted to tube facies so as to connect the cell faces. This process created a face-connected tube feature from the onshore to the offshore setting, allowing simulated groundwater flow to occur continuously through the feature. The filling-in process increased the width and thickness of the lava tubes but kept them within known ranges of lava tube height and width (Cooper and Kauhikaua, 1992). Due to the additional cells, the lava tube facies percentage nearly doubled (from 3% to 6%), and the aa percentage was reduced by a corresponding amount (~3%) compared to the initial output.

A second set of heterogeneous models were created to represent systems with different geometry of geologic structure than those of the conduit models. Indicator variograms were calculated for each facies and 3-D direction for each conduit realization. Variogram models similar, but not identical, to each of these were used in sequential indicator simulations (SIS) conducted in SGeMS (Remy et al., 2009) on the same grid as that of the conduit models. SIS uses separate variograms for each facies to create a field that has the same approximate facies percentages and the same

distance-based statistics as an original input field but without any of the geometrical continuity. Seven SIS models were produced from this, each of which corresponded approximately to an original conduit model. Variogram model parameters are given in Table 2.

Table 2 Parameter values used in variogram models for each geologic facies.

Note that the exponential variogram model, $\gamma(h) = C(1 - e^{-\frac{h}{a_h}})$, was adopted in SIS simulations, where C is sill, a_h is range, and h is the distance between each pair of points.

R#	Tube		Aa		Transitional		Clinker		Pahoehoe		Ash	
	C [-]	a_h [m]	C [-]	a_h [m]	C [-]	a_h [m]	C [-]	a_h [m]	C [-]	a_h [m]	C [-]	a_h [m]
Across-shore direction												
1	0.07	51	0.18	42	0.045	33	0.085	30	0.112	66	0.00026	15
2	0.05	51	0.19	27	0.037	30	0.06	24	0.055	21	0.0003	18
3	0.046	33	0.21	21	0.038	40	0.098	30	0.098	27	0.00028	15
4	0.09	51	0.23	30	0.041	36	0.077	27	0.07	120	0.00028	18
5	0.055	39	0.215	39	0.028	27	0.088	48	0.1	63	0.00083	18
6	0.092	39	0.235	27	0.028	24	0.084	18	0.133	42	0.00048	18
7	0.082	39	0.225	30	0.023	33	0.045	54	0.11	39	0.00082	18
Along-shore direction												
1	0.07	51	0.18	48	0.045	33	0.085	33	0.112	72	0.00026	15
2	0.05	51	0.19	27	0.037	30	0.06	33	0.055	36	0.0003	18
3	0.046	33	0.21	33	0.038	40	0.098	30	0.098	39	0.00028	15
4	0.09	51	0.23	36	0.041	36	0.077	27	0.07	102	0.00028	18
5	0.055	39	0.215	42	0.028	27	0.088	51	0.1	63	0.00083	18
6	0.092	39	0.235	27	0.028	24	0.084	21	0.133	48	0.00048	18
7	0.085	39	0.225	36	0.023	33	0.045	60	0.11	39	0.00082	18
Vertical direction												
1	0.07	10	0.18	5	0.045	6	0.085	6	0.112	5	0.00026	3
2	0.05	10	0.19	3	0.037	6	0.06	5	0.055	3	0.0003	3
3	0.046	6	0.21	4	0.038	6	0.098	6	0.098	4	0.00028	3
4	0.09	10	0.23	5	0.041	7	0.077	5	0.07	14	0.00028	4
5	0.055	8	0.215	7	0.028	5	0.088	7	0.1	8	0.00083	3
6	0.092	8	0.235	5	0.028	5	0.084	4	0.133	4	0.00048	4
7	0.085	8	0.225	4	0.023	6	0.045	11	0.11	4	0.00082	4

A hydraulic conductivity value was assigned to each facies type in the heterogeneous models (conduit and SIS) for use in the flow and transport models (Table 1). Values were selected for each facies within established ranges in the literature. The K value of transitional lava is not well established and was chosen to be between aa and pahoehoe. The K value for lava tubes was chosen to be two orders of magnitude higher than the next highest K (i.e., clinker) to better establish a dominant flow feature.

Homogeneous realizations with equivalent horizontal and vertical K were also generated for each realization of the conduit simulations. This was done by simulating groundwater flow horizontally and vertically through each realization and then calculating K from the simulated flow using Darcy's Law. To calculate horizontal K, head boundaries of 1.5m and 0m were applied on the landward and seaward boundaries, with no-flow boundaries on the other sides. To calculate vertical K, the top and bottom boundaries. Groundwater flow rate through the model was calculated and used to calculate K for each direction for each realization. Domain discretization was equivalent to that of the heterogeneous models.

Numerical groundwater models were developed in 3D using SEAWAT (Guo and Langevin, 2002) to simulate density-dependent groundwater flow and salt transport. Figure 1 shows the model size and discretization. A distance of 500m from the shoreline was set as the location of the landward boundary due to computational constraints on the model size. Head values 500m inland from the coastline range from 0.5m to 1.5m depending on location within the study area (NWIS, 2017). However, heads in other nearshore areas around Hawaii reach up to 4m. A head boundary of

2.5m was chosen to approximate generally representative shoreline conditions while still being high enough to drive groundwater flow to steady-state within a reasonable timeframe. The offshore boundary extended 500m offshore so that 1) the seaward boundary did not interfere with the mixing zone; and 2) the groundwater discharge could extend offshore, as observed in previous studies. A constant head value of 0m was assigned to the offshore top and vertical boundaries. All other boundaries were no-flow. Transport boundary conditions were constant concentration of 0g/L along the landward vertical boundary and 35g/L along the offshore top and vertical boundaries. All other boundaries were zero flux.

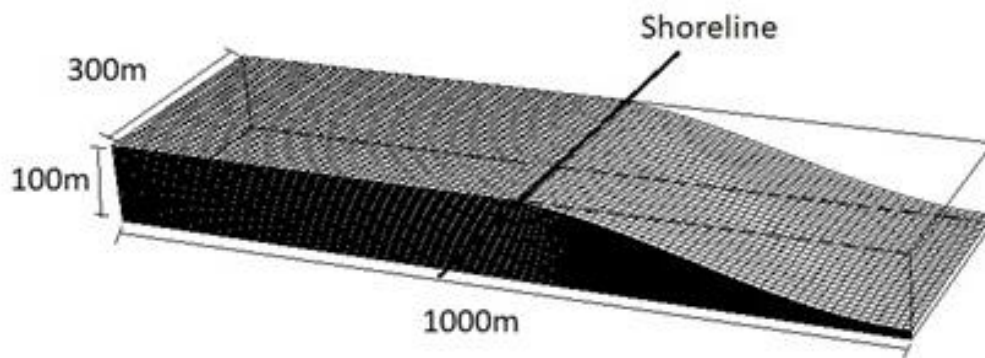


Figure 1 SEAWAT model domain.

All SEAWAT simulations were run until both flowfields and salinity distributions reached steady state, and results were quantified by several metrics. The *inland extent of saline water* is the farthest inland location with a salinity of 35ppt.

The *offshore extent of freshwater* is the farthest offshore location with salinity of <1 ppt. *Mixing zone volume* is the volume of the domain containing cells between 10% and 90% seawater salinity. *Mixing zone center of mass* for the cross-shore directions is the center of mass of that volume in the x-direction for a given row (from onshore boundary to offshore boundary) of the model domain, averaged over the rows:

$$x_{center} = \frac{\sum_{i=1}^n m_i x_i}{\sum_{i=1}^n m_i}$$

where m_i is equal to the salinity value of a given cell along the row, and x_i is equal to the x-coordinate of that same cell.

The *ratio of saline to fresh SGD* relates the magnitude of saline recirculation to fresh throughflow and is an indicator of total SGD. *Variability in SGD* was characterized as the variance of discharge along every row in the alongshore direction for the length of the offshore domain.

Chapter 3

RESULTS

Simulation results show substantial differences in subsurface salinity distributions among the three geologic model types. Conduit models displayed complex salinity distributions that differed substantially from the more typical saltwater wedges of the equivalent homogeneous simulations (Figure 2a). Salinity in the conduit simulations varied in the alongshore direction and exhibited both fresh and saline water in locations not consistent with equivalent homogeneous systems. Salinity distribution varied not only from the other two model types but within each conduit realization as well. As observed in Figure 2a, the salinity at 270m across differs from the salinity at 120m across. The other two model types have similar salinity distributions regardless of location along the shoreline. The SIS models had mixing zone distributions generally extending inland from the shoreline, similar to the standard saltwater wedge of homogeneous simulations but slightly more irregular and wider (Figure 2c, e). Appendix D contains results for all realizations.

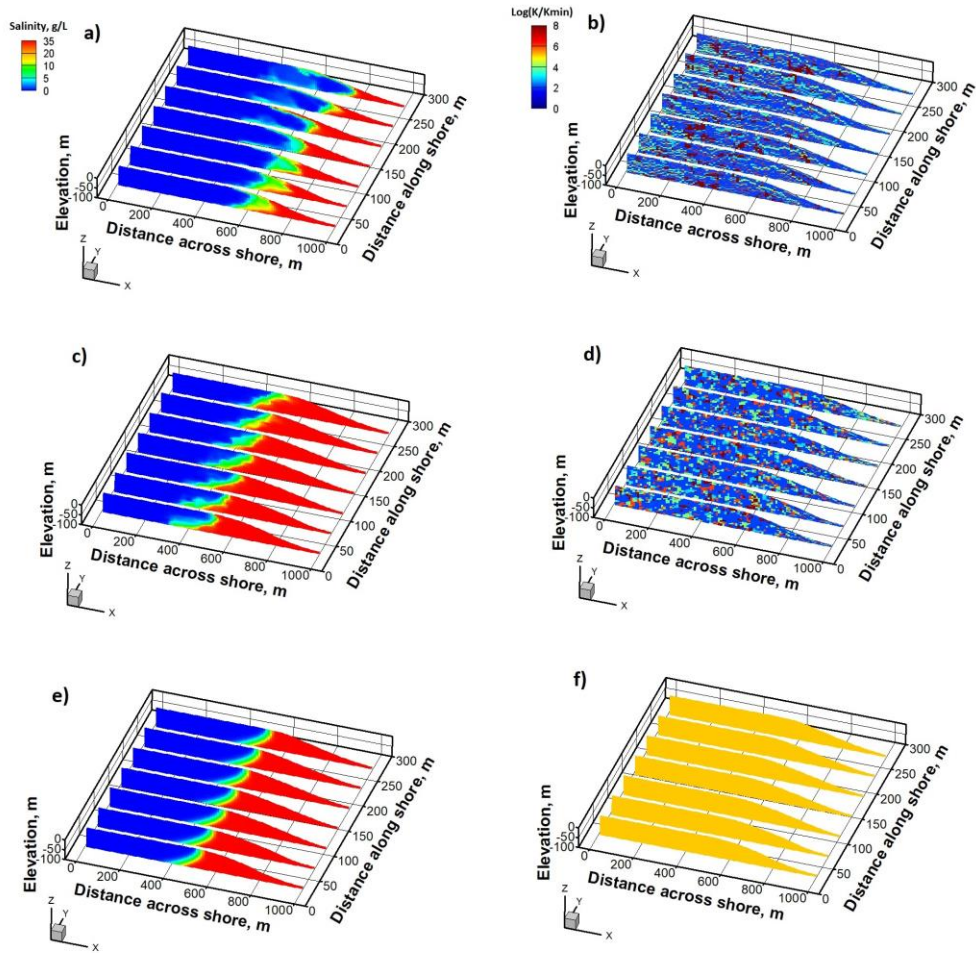


Figure 2 Normalized hydraulic conductivity fields (b, d, f) and salinity distributions (a, c, e) for selected conduit (a, b), SIS (c, d) and homogeneous (e, f) realizations.

The brackish water mass in the conduit models extended farther offshore in every case compared to the homogeneous models (Figure 3 (top); Figure 4a, c, e). The error bars in Figure 3 indicate the wide distribution of the location of the mixing zone in conduit cases. In homogeneous cases, the brackish extent was the same regardless

of alongshore location. Both onshore saline extent and offshore freshwater extent were further seaward for conduit cases compared to equivalent homogeneous cases for all but one realization, and in some cases by several hundred meters (Figure 3 middle, bottom).

The homogeneous models displayed differing onshore extents depending on the anisotropy in K (K_h/K_v) of the model. Realizations with higher ratios had a larger onshore extent of saline water (see Appendix C). For four of the models, the onshore extent ended at 420m inland from the coastline. These four models had horizontal hydraulic conductivities in the vicinity of 1×10^{-4} m/s. The other three models had onshore saline water that only extended 260 to 360m onshore. These models had either horizontal or vertical hydraulic conductivities that were one or two orders of magnitude below the other four. Since both horizontal and vertical K can influence the landward position of the wedge, the ratio of horizontal to vertical is the important factor in determining the wedge position. In the conduit cases, the landward extent of saline water was less than in homogeneous cases in every realization but one. Since the homogeneous models were derived from the conduit models, the effective hydraulic conductivities are the same. As such, the specific geometry of the geology in the conduit models is responsible for the difference in wedge location.

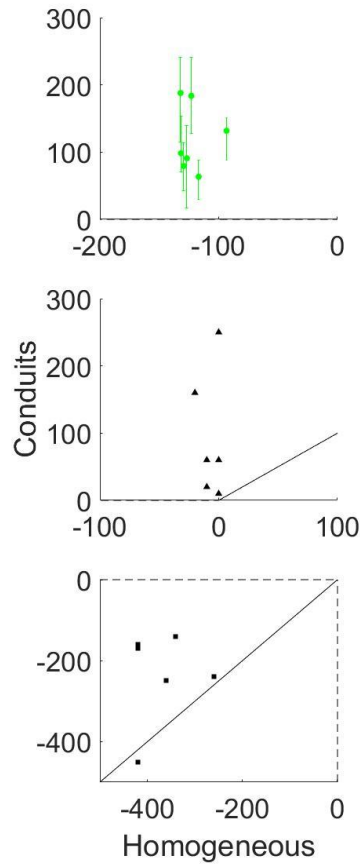


Figure 3 Average x-location (in meters) of centers of mass of brackish ($1 < \text{ppt} < 34$) body (top panel), onshore extent of saline water (middle panel), and offshore extent of freshwater (bottom panel) for each homogeneous and conduit model realization. Error bars in the top panel represent range of body extents across all cross-sections in conduit cases. Error bars for homogeneous cases were minimal.

The total volume of the mixing zone was higher on average in conduit cases than both homogeneous and SIS cases (Figure 4a). Of the seven conduit realizations, the largest mixing zone volume was an order of magnitude greater than the other mixing zones across all systems. However, the smallest conduit mixing zone volume

was less than the average SIS volume. This shows that, while on the whole conduit cases have a larger mixing zone than other cases, there is a large amount of variability in the volume that depends on the specific geometry of a given case. The horizontal position of the mixing zone center of mass for conduit cases was on average 120m offshore. SIS and homogeneous cases had mixing zones that were, on average, centered 40m and 120m onshore of the shoreline, respectively. As with total volume, the location of the center of mass of conduit model mixing zones was more variable than the other cases, ranging from the shoreline to 250m offshore.

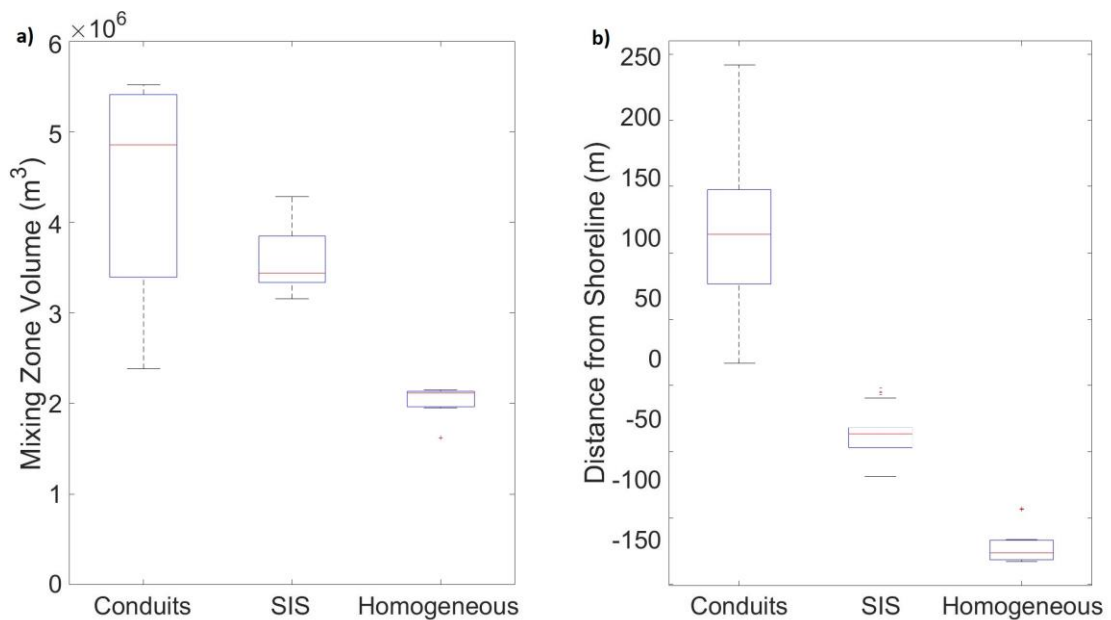


Figure 4 Average mixing zone volume (a) and center of mass x-location (b) across all realizations. Red lines indicate the median data value. Top and bottom of the rectangles represent the 25th and 75th percentile of the dataset, and error bars indicate maximum and minimum volume and extent, respectively. Red crosses indicate potential outlier data.

The offshore groundwater discharge and recharge patterns differed among the three aquifer types (Figure 5). In homogeneous models, groundwater discharge was focused at the shoreline and recharge occurred offshore. In heterogeneous models, discharge rates were generally higher at the shoreline than offshore, but discharge extended farther offshore, more so in the conduit cases compared to SIS cases. In SIS simulations, few discharge cells were present farther than 100m offshore and recharge occurred relatively uniformly across the offshore domain, despite the presence of lava tube facies. There were a few high-volume discharge cells in the nearshore (within 10m of shoreline) for SIS cases, which are likely due to clusters of high-K cells. Because there is not the same level of connectivity as in conduit cases, however, the high discharge is not found further offshore. In the conduit simulations, focused patterns of both discharge and saltwater recharge corresponding to lava tubes were apparent (Figure 5). Individual cells of high discharge appear at the model surface next to individual cells of high recharge. These high recharging cells exist in an otherwise low recharge area or an area of no recharge at all. When the high discharge and recharge cells are physically close to each other in the conduit cases, a small circulation cell is developed with high volume. These circulation cells are not seen in either SIS or homogeneous models.

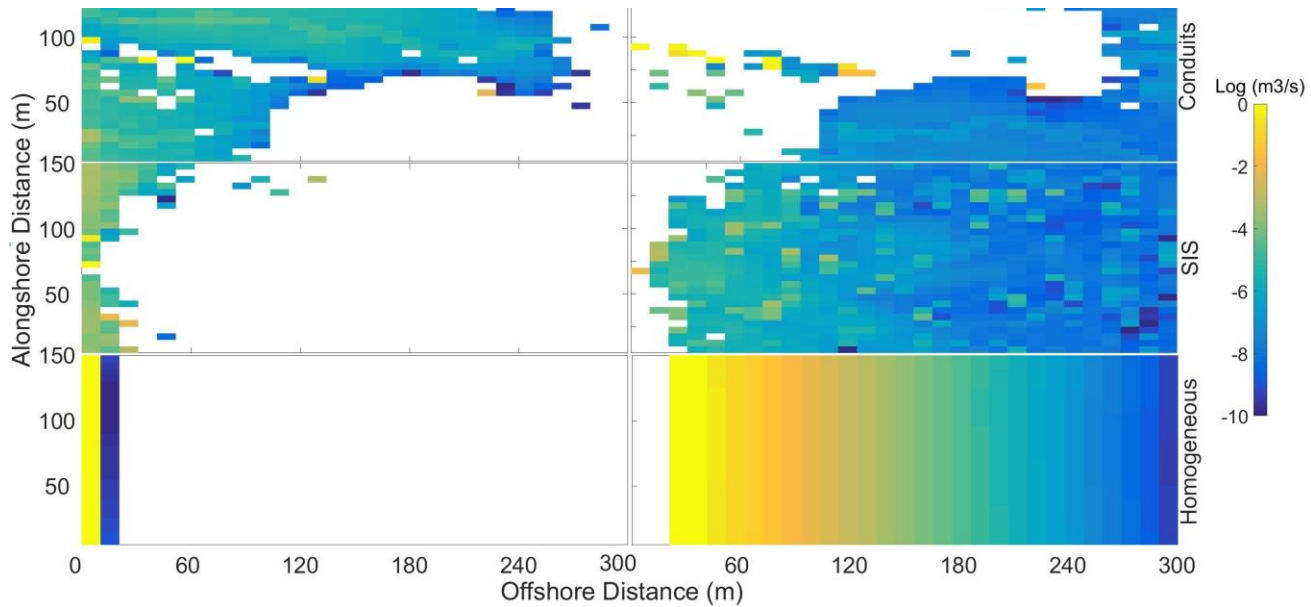


Figure 5 SGD (left) and SGR (right) values for conduit (top), homogeneous (center), and SIS (bottom) realizations. Shoreline is at the leftmost boundary of plots.

The variability of flux in the alongshore direction was much greater over a larger offshore area in the conduit cases than in either the homogeneous or SIS cases (Figure 6). Homogeneous and SIS cases both had variance spikes at the shoreline, where discharge was concentrated. The homogeneous shoreline spike was seven orders of magnitude lower than the SIS spike. The conduit cases had high variance of similar magnitude to SIS across the offshore domain up to a distance of approximately 150m. As was the case with salinity distribution with depth, the conduit cases have more alongshore variability with surface discharge as well.

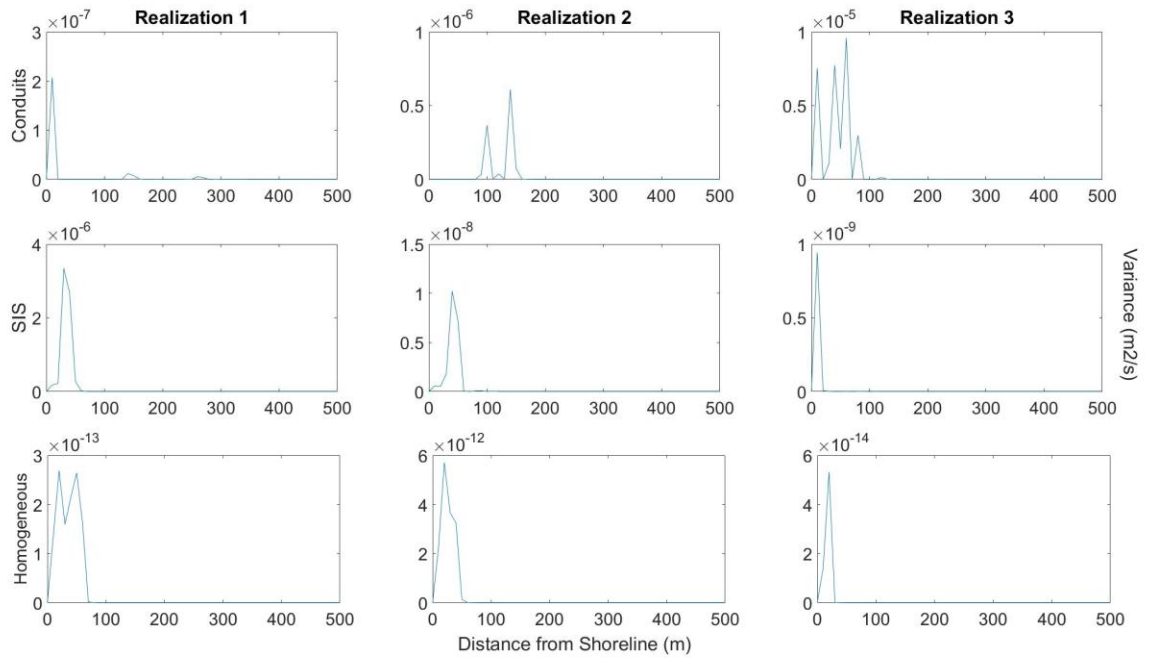


Figure 6 Flux variance in the transverse alongshore direction for conduit (top), homogeneous (center), and SIS (bottom) models for three example realizations.

Total fresh and saline SGD varied among the model types (Figure 7). On average, fresh discharge was greatest in homogeneous models, but variability was greatest in conduit models. Fresh discharge in conduit and homogeneous models was equivalent on average due to the constant flow boundary in the homogeneous model. SIS models had low average fresh discharge and low variability. The difference in average fresh discharge (and therefore fresh inflow) could be due to a lack of equivalence in effective permeability (conduit and homogeneous models have equivalent effective K values, whereas SIS models do not). Saline discharge, or saltwater circulation driven by subsurface density gradients, was greatest in conduit

models, followed by SIS and homogeneous models. Variability was high in both types of heterogeneous models and low in homogeneous models.

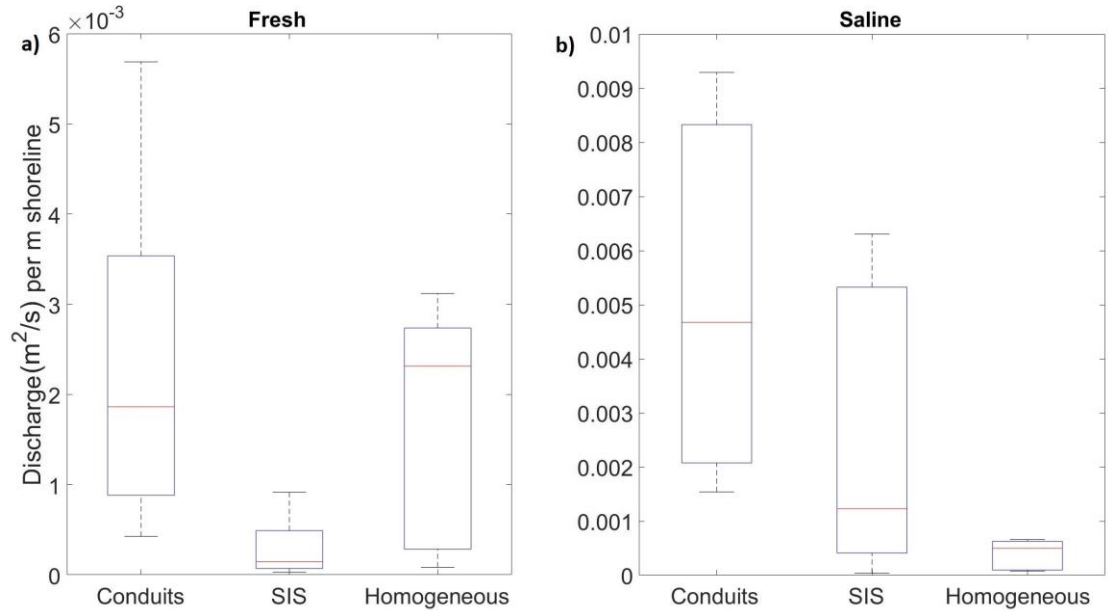


Figure 7 Comparison of average fresh (a) and saline (b) discharge rates across model domains. Error bars indicate maximum and minimum values across seven realizations.

The ratio of saline to fresh SGD was greater than 1 in all but one heterogeneous case and was as high as 32. The ratio was nearly uniformly greater in both types of heterogeneous cases compared to the equivalent homogeneous cases (Figure 8), and the conduit and SIS cases displayed similar ratios on average. This is likely because salinity distributions are complex in both conduit and SIS cases, leading

to multiple density-driven circulation cells and high saline to fresh SGD ratios, as shown in previous studies (Michael et al., 2016), compared to a monotonic distribution and thin mixing zone in homogeneous cases.

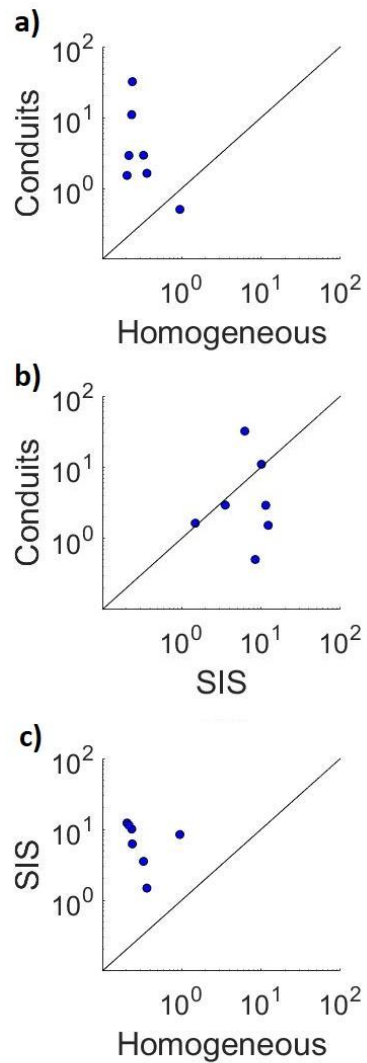


Figure 8 Comparison of the saline SGD/fresh SGD ratio between model simulations.

The conduit cases, as a whole, contained more discharging cells than either the SIS or homogeneous cases (Figure 9). The majority of these cells discharged between 10^{-4} and 10^{-5} m³/s of water. The SIS cases displayed a similar range of discharging cells, but the number of cells was much smaller for each volume. The homogeneous cases displayed a range of discharge that was higher than both heterogeneous cases (between 10^{-2} and 10^{-3}) but had a lower number of discharging cells as in the conduit case. Additionally, SIS cases contained the highest volume discharge cells, with some coming close to 10 m³/s. The number of cells that discharged high volumes was comparatively small, but homogeneous and conduit cases did not display any cells with similar volumes.

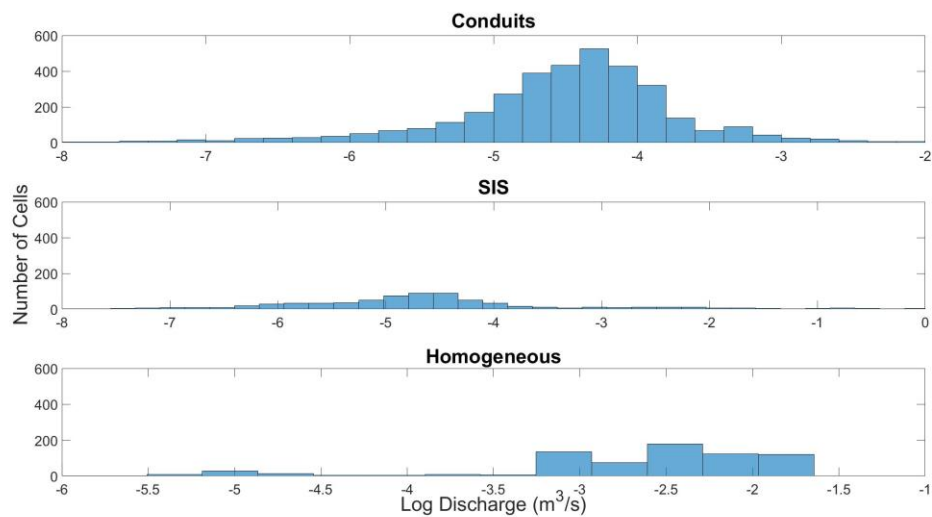


Figure 9 Histograms of log discharge for all conduit, SIS, and homogeneous cases.

Chapter 4

DISCUSSION

Through comparison of two types of heterogeneity - with and without conduits but with similar facies proportions - we demonstrate that geologic structure is a critical factor in determining salinity distributions in coastal aquifers. In our set of simulations, salinity patterns in conduit cases were highly variable and mixing zones far offshore, compared to more typical wedge-type mixing zones in the SIS and homogeneous cases. This is a somewhat different result from Michael et al. (2016), who showed that salinity distributions in SIS-generated heterogeneous aquifers can differ substantially from equivalent homogeneous simulations for models with highly continuous facies in the across-shore direction. The extent to which SIS-type heterogeneous geometries result in complex salinity distributions similar to those of our conduit models likely depends on the extent of onshore to offshore facies continuity compared to model extent. For our simulations, the SIS variogram ranges were 15m to 40m depending on the realization and facies, which was 1.5% to 4% of the total domain length. In Michael et al. (2016), variogram range for high-continuity models was 50km, which was 25% of the domain length, whereas the low-continuity models had a variogram range of only 5km, 5% of the domain length. Similarly to our SIS simulations, the low-continuity SIS simulations of Michael et al. (2016) had salinity distributions similar to, but slightly more variable than, the equivalent homogeneous simulations. Thus, it is important to accurately understand and model the degree of connectivity in a system relative to domain size.

Another factor that is likely to affect salinity and SGD in coastal aquifers is the proportion of high-K and low-K facies. For example, the models of Michael et al.

(2016) ranged from 20.5% clay to 16.0% coarse sand. This contrasts with our facies ranging from 75% a'a to 3% lava tube. The large proportion of low-K facies and the disconnected nature of higher-K facies may also contribute to the differences between the SIS heterogeneity in our results and the heterogeneity in prior studies.

Heterogeneous models, particularly the conduit cases, have more complex salinity distributions than homogeneous models. These complex density gradients drive more saline groundwater convection, resulting in greater saline SGD. Comparison of the ratio of saline SGD to fresh SGD (Figure 8) among the three cases shows that the conduit simulations consistently conducted more saline circulation than either the homogeneous or SIS simulations. Figures 7 and 9 show that conduit cases have the highest volume of fresh and saline water as well as the highest number of discharging cells. This all indicates that regardless of specific geometry, a conduit system will have a higher total discharge, larger distribution of discharge, and higher saline recirculation than either homogeneous or SIS-type systems. Knowing this influences the methods by which such systems are studied and should also inform the amount of data that needs to be collected before such a system can be properly analyzed.

The modeling results indicate that in systems like Hawaii where connected conduits are present, care must be taken in designing coastal field studies to overcome the high degree of heterogeneity of both salinity and SGD. Because the variance in SGD in conduit models was orders of magnitude greater than the SIS and homogeneous counterparts, a large number of measurements are necessary to sufficiently characterize SGD. The complex salinity distributions present a similar challenge, and would require a greater number of measurements or different non-point

approaches for characterization and management. When focusing on regions that have continuous connected features, best practices for characterization should include multiple measurement methods. Similar conclusions can be drawn for other aquifer systems with continuous geologic features such as karstic fractures or paleochannels. Systems with similar geometry of geologic features to an SIS simulation could include deltas or glacial fields. An understanding of the underlying geometry of the system should inform the type, locations, and number of measurements for coastal aquifer system characterization.

The distance that fresh groundwater extends offshore and that saline groundwater extends inland are important for water resources assessment (Cohen et al., 2010; Post et al., 2013; Knight et al., 2018). As sea level and populations rise, saltwater intrusion will be an increasing problem for coastal communities, and knowledge of how and where the intrusion is likely to occur and the volume of fresh water available for extraction could greatly aid in mitigation efforts. The continuous, high-K conduits in our simulations conduct fresh groundwater farther offshore than heterogeneous systems with less-connected geometry or homogeneous aquifers. Additionally, saline groundwater in the lava tube system did not extend as far inland as in homogeneous cases, indicating that conduit systems may have more of a buffer against seawater intrusion. However, these high-K conduits can also allow fast preferential flow inland in response to pumping. More work is necessary to better characterize transient responses to human perturbations and hydrologic change.

Chapter 5

CONCLUSION

Coastal groundwater systems are important resources for island communities. In some cases, the entirety of the freshwater supply comes from groundwater, and understanding how and where it discharges is necessary for proper management. In addition, knowledge of seawater recirculation and mixing zone dynamics is crucial for understanding geochemical reactions that are affected by such processes.

In volcanic aquifers, lava tubes can act as conduits for groundwater in a less permeable matrix of lava flows. Such preferential flow can have an important impact on groundwater salinity distributions and SGD. In order to understand the importance of such conduits, we conducted a comparative study with different types of geologic systems.

The salinity and flux distributions in three types of aquifer geometry show that discharge patterns differ based on the degree and nature of heterogeneity present in the model. Conduit realizations had more unique salinity distributions and, in general, a farther offshore discharge of fresh and brackish water than homogeneous or SIS realizations. Systems with conduits also had larger mixing zones with centers of mass farther offshore than in other cases. Conduits also contributed to higher point-source fluxes of both fresh and saline water and greater density-driven circulation of saline groundwater. The variance of flux across the surface of the models was highest in the conduit cases and lower in the SIS and homogeneous cases.

These results provide an explanation for brackish, offshore plumes found on the western coast of Hawaii. They also indicate a need for multiple points and methods of sampling in areas where conduit-type, heterogeneous geology is expected to occur

in a coastal setting. Closer inspection is necessary in locations demonstrating conduit-like discharge in order to examine exactly what the geology looks like where the discharge is occurring. In addition, larger models of different study sites should be created to observe whether similar discharge and recharge patterns emerge in areas with different lava flow geometries and on larger scales.

REFERENCES

- Almasri, M.N. (2008). Assessment of intrinsic vulnerability to contamination for Gaza coastal aquifer, Palestine. *Journal of Environmental Management*, 88.4: 577-593.
- Anderson, S.R., Kuntz, M.A., and Davis, L.C. (1999). Geologic controls of hydraulic conductivity in the Snake River Plain Aquifer at and near the Idaho National Engineering and Environmental Laboratory, Idaho. U.S. Geological Survey Water-Resources Investigation Report 99-4033. Bauer, R.D., Rolle, M., Bauer, S., Eberhardt, C., Grathwohl, P., Kolditz, O., Meckenstock, R.U., and Griebler, C. (2009). Enhanced biodegradation by hydraulic heterogeneities in petroleum hydrocarbon plumes. *Journal of Contaminant Hydrology*, 105: 56-68.
- Barlow, P.M. and Reichard, E.G. (2010). Saltwater intrusion in coastal regions of North America. *Hydrogeology Journal*, 18.1: 247-260.
- Bear, J., Cheng, A. H.-D., Sorek, S., Ouazar, D., and Herrera, I. (1999). Seawater intrusion in coastal aquifers: Concepts, methods, and practices.
- Bianchi, M., Zheng, C., Wilson, C., Tick, G.R., Liu, G., and Gorelick, S.M. (2011). Spatial connectivity in a highly heterogeneous aquifer: From cores to preferential flow paths. *Water Resources Research*, 47: W05524.
- Bishop, J.M., Glenn, C.R., Amato, D.W., and Dulai, H. (2017). Effect of land use and groundwater flow path on submarine groundwater discharge nutrient flux. *Journal of Hydrology: Regional Studies*, 11: 194-218.
- Böhlke, J.K. and Denver, J.M. (1995). Combined use of groundwater dating, chemical, and isotopic analyses to resolve the history and fate of nitrate contamination in two agricultural watersheds, Atlantic Coastal Plain, Maryland. *Water Resources Research*, 31: 2319-2339.
- Burnett, W.C., Wattayakorn, G., Taniguchi, M., Dulaiova, H., Sojisuporn, P., Rungsupa, S., and Ishitobi, T. (2007). Groundwater-derived nutrient inputs to the Upper Gulf of Thailand. *Continental Shelf Research*, 27: 176-190.
- Burnett, W.C., Aggarwal, P.K., Aureli, A., Bokuniewicz, H., Cable, J.E., Charette, M.A., Kontar, E., Krupa, S., Kulkarni, K.M., Loveless, A., Moore, W.S., Oberdorfer, J.A., Oliveira, J., Ozyurt, N., Povinec, P., Privitera, A.M.G., Rajar, R., Ramessur, R.T., Scholten, J., Stieglitz, T., Taniguchi, M., and Turner, J.V. (2006). Quantifying submarine groundwater discharge in the coastal zone via multiple methods. *Sciences of the Total Environment*, 367.2-3: 498-543.

- Burnett, W.C., Bokuniewicz, H., Huettel, M., Moore, W.S., and Taniguchi, M. (2003). Groundwater and pore water inputs to the coastal zone. *Biogeochemistry*, 66: 3-33.
- Bussman, I. and Suess, E. (1998). Groundwater seepage in Eckernförde Bay (Western Baltic Sea): Effect on methane and salinity distribution of the water column. *Continental Shelf Research*, 18: 1795-1806.
- Cherkauer, D.S. and Nader, D.C. (1989). Distribution of groundwater seepage to large surface-water bodies: The effect of hydraulic heterogeneities. *Journal of Hydrology*, 109: 151-165.
- Cohen, D., Person, M., Wang, P., Gable, C.W., Hutchinson, D., Marksamer, A., Dugan, B., Kooi, H., Groen, K., and Lizarralde, D. (2010). Origin and extent of fresh paleowaters on the Atlantic continental shelf, USA. *Ground Water*, 48: 143-158.
- Comte, J.-C., Wilson, C., Ofterdinger, U., and González-Quirós, A. (2017). Effect of volcanic dykes on coastal groundwater flow and saltwater intrusion: A field-scale multiphysics approach and parameter evaluation. *Water Resources Research*, 53.3: 2171-2198.
- Cruz, J.V. and Silva, M.O. (2000). Groundwater salinization in Pico Island (Azores, Portugal): origin and mechanisms. *Environmental Geology*, 39: 1181-1189.
- Cushman, J.H., Hu, B.X., and Deng, F.-W. (1995). Nonlocal reactive transport with physical and chemical heterogeneity: Localization errors. *Water Resources Research*, 31.9: 2219-2237.
- DeSimone, L.A. and Howes, B.L. (1996). Denitrification and nitrogen transport in a coastal aquifer receiving wastewater discharge. *Environmental Science and Technology*, 30: 1152-1162.
- Ducci, D. (2010). Aquifer vulnerability assessment methods: The non-independence of parameters problem. *Journal of Water Resource and Protection*, 2: 298-308.
- Fabricius, K.E. (2005). Effects of terrestrial runoff on the ecology of corals and coral reefs: Review and synthesis. *Marine Pollution Bulletin*, 50: 125-146.
- Fornari, D.J. (1986). Submarine lava tubes and channels. *Bulletin of Volcanology*, 48: 291-298.

- Garcia, M.O., Haskins, E.H., Stolper, E.M., and Baker, M. (2007). Stratigraphy of the Hawai'i Scientific Drilling Project core (HSDP2): Anatomy of a Hawaiian shield volcano. *Geochemistry Geophysics Geosystems*, 8.2, Q02G20, doi: 10.1029/2006GC001379.
- Giambastiani, B.M.S., Antonellini, M., Essink, G.H.P.O., and Stuurman, R.J. (2007). Saltwater intrusion in the unconfined coastal aquifer of Ravenna (Italy): A numerical model. *Journal of Hydrology*, 340.1-2: 91-104.
- Gingerich, S.B., and Voss, C.I. (2005). Three-dimensional variable-density flow simulation of a coastal aquifer in southern Oahu, Hawaii, USA. *Hydrogeology Journal*, 13: 436-450.
- Goebel, M., Pidlisecky, A., and Knight, R. (2017). Resistivity imaging reveals complex pattern of saltwater intrusion along Monterey coast. *Journal of Hydrology*, 551: 746-755.
- Greeley, R. (1971). Observations of actively forming lava tubes and associated structures, Hawaii. NASA Technical Memorandum X-62,014.
- Guo, W. and Langevin, C.D. (2002). User's guide to SEAWAT; a computer program for simulation of three-dimensional variable-density ground-water flow. U.S. Geological Survey Techniques of Water-Resources Investigations 06-A7.
- Hendrickx, J.M.H. and Flury, M. (2001). Uniform and preferential flow mechanisms in the vadose zone. *Conceptual Models of Flow and Transport in the Fractured Vadose Zone*. National Academy Press, Washington, D.C.
- Hon, K., Kauahikaua, J., Denlinger, R., and Mackay, K. (1994). Emplacement and inflation of pahoehoe sheet flows: Observations and measurements of active lava flows on Kilauea Volcano, Hawaii. *GSA Bulletin*, 106.3: 351-370.
- Hu, B.X., Meerschaert, M.M., Barrash, W., Hyndman, D.W., He, C., Li, X., and Guo, L. (2009). Examining the influence of heterogeneous porosity fields on conservative solute transport. *Journal of Contaminant Hydrology*, 108.3-4: 77-88.
- Hunt, Jr., C.D., Ewart, C.J., and Voss, C.I. (1988). Region 27, Hawaiian islands, *in* Seaber, P.R., ed., *Hydrogeology: Boulder, Colorado*, Geological Society America, *Geology of North America*, v. 0-2, p. 255-262.
- Huyakorn, P.S., Andersen, P.F., Mercer, J.W., and White Jr., H.O. (1987). Saltwater intrusion in aquifers: Development and testing of a three-dimensional finite element model. *Water Resources Research*, 23.2: 293-312.

- Hwang, D.-W., Kim, G., Lee, Y.-W., Yang, H.-S. (2005). Estimating submarine inputs of groundwater and nutrients to a coastal bay using radium isotopes. *Marine Chemistry*, 96: 61-71.
- Hwang, D.-W., Lee, Y.-W., and Kim, G. (2005). Large submarine groundwater discharge and benthic eutrophication in Bangdu Bay on volcanic Jeju Island, Korea. *Limnology and Oceanography*, 50: 1393-1403.
- Johnson, A.G., Glenn, C.R., Burnett, W.C., Peterson, R.N., and Lucey, P.G. (2008). Aerial infrared imaging reveals large nutrient-rich groundwater inputs to the ocean. *Geophysical Research Letters*, 35, L15606, doi: 10.1029/2008GL034574.
- Kalbus, E., Schmidt, C., Molson, J.W., Reinstorf, F., and Schirmer, M. (2009). Influence of aquifer and streambed heterogeneity on the distribution of groundwater discharge. *Hydrology and Earth System Sciences*, 13: 69-77.
- Kerrou, J. and Renard, P. (2010). A numerical analysis of dimensionality and heterogeneity effects on advective dispersive seawater intrusion processes. *Hydrogeology Journal*, 18: 55-72.
- Kim, Y., Lee, K.-S., Koh, D.-C., Lee, D.-H., Lee, S.-G., Park, W.-B., Koh, G.-W., Woo, N.-C. (2003). Hydrogeochemical and isotopic evidence of groundwater salinization in a coastal aquifer: a case study in Jeju volcanic island, Korea. *Journal of Hydrology*, 270: 282-294.
- Knight, A.C., Werner, A.D., and Morgan, L.K. (2018). The onshore influence of offshore fresh groundwater. *Journal of Hydrology*, 561: 724-736.
- Koeppen, W.C., Patrick, M., Orr, T., Sutton, A.J., Dow, D., and Wright, R. (2013). Constraints on the partitioning of Kilauea's lavas between surface and tube flows, estimated from infrared satellite data, sulfur dioxide emission rates, and field observations. *Bulletin of Volcanology*, 75:716.
- Koneshloo, M., Kreyns, P., and Michael, H.A. (2018). Combining process-based and surface-based models to simulate subsurface heterogeneity in volcanic aquifers. *Stochastic Environmental Research and Risk Assessment*, 32: 2565-2583.
- Kroeger, K.D., Swarzenski, P.W., Greenwood, W.J., and Reich, C. (2007). Submarine groundwater discharge to Tampa Bay: Nutrient fluxes and biogeochemistry of the coastal aquifer. *Marine Chemistry*, 104: 85-97.

- Kung, K.-J. S. (1990). Preferential flow in a sandy vadose zone: 2. Mechanism and implications. *Geoderma*, 46: 59-71.
- Lapointe, B.E. and Matzie, W.R. (1996). Effects of stormwater nutrient discharges on eutrophication processes in nearshore waters of Florida keys. *Estuaries*: 19: 422-435.
- Lee, Y.-W., Kim, G., Lim, W.-A., Hwang, D.-W. (2009). A relationship between submarine groundwater borne nutrients traced by Ra isotopes and the intensity of dinoflagellate red-tides occurring in the southern sea of Korea. *Limnology and Oceanography*, 55.1: 1-10.
- Lee, Y.-W., and Kim, G. (2007). Linking groundwater-borne nutrients and dinoflagellate red-tide outbreaks in the southern sea of Korea using a Ra tracer. *Estuarine, Coastal, and Shelf Science*, 71: 309-317.
- Li, L., Barry, D.A., Stagnitti, F., and Parlange, J.-Y. (1999). Submarine groundwater discharge and associated chemical input to a coastal sea. *Water Resources Research*, 35: 3253-3259.
- Li, X., Hu, B.X., Burnett, W.C., Santos, I.R., and Chanton, J.P. (2009). Submarine ground water discharge driven by tidal pumping in a heterogeneous aquifer. *Groundwater*, 47.4: 558-568.
- Macdonald, G.A. (1972). *Volcanoes*. Prentice-Hall Inc., Englewood Cliffs, 510 pp.
- Melloul, A.J. and Goldenberg, L.C. (1997). Monitoring of seawater intrusion in coastal aquifers: Basics and local concerns. *Journal of Environmental Management*, 51: 73-86.
- Michael, H.A., Scott, K.C., Koneshloo, M., Yu, X., Khan, M.R., and Li, K. (2016). Geologic influence on groundwater salinity drives large seawater circulation through the continental shelf. *Geophysical Research Letters*, 43.20: 10,782-10,791.
- Michael, H.A., Russoniello, C.J., and Byron, L.A. (2013). Global assessment of vulnerability to sea-level rise in topography-limited and recharge-limited coastal groundwater systems. *Water Resources Research*, 49: 2228-2240.
- Michael, H.A., Lubetsky, J.S., and Harvey, C.F. (2003). Characterizing submarine groundwater discharge: A seepage meter study in Waquoit Bay, Massachusetts. *Geophysical Research Letters*, 30.6: 1297.

- Miller, J.A., Whitehead, R.L., Gingerich, S.B., Oki, D.S., and Olcott, P.G. (2000). Ground water atlas of the United States. USGS Hydrologic Atlas 730. N1-N36.
- Moore, W.S. (2010). The effect of submarine groundwater discharge on the ocean. *Annual Review of Marine Science*, 2: 59-88.
- Moore, W.S., Krest, J., Taylor, G., Roggenstein, E., Joye, S., and Lee, R. (2002). Thermal evidence of water exchange through a coastal aquifer: Implications for nutrient fluxes. *Geophysical Research Letters*, 29: 1704.
- Moore, W.S. (1999). The subterranean estuary: A reaction zone of ground water and sea water. *Marine Chemistry*, 65: 111-125.
- Moore, W.S. (1996). Large groundwater inputs to coastal waters revealed by ²²⁶Ra enrichments. *Nature*, 380: 612-614.
- Mulligan, A.E., Evans, R.L., and Lizarralde, D. (2006). The role of paleochannels in groundwater/seawater exchange. *Journal of Hydrology*, 335: 313-329.
- Mulrennan, M.E. and Woodroffe, C.D. (1998). Saltwater intrusion into the coastal plains of the Lower Mary River, Northern Territory, Australia. *Journal of Environmental Management*, 54: 169-188.
- National Centers for Environmental Information (NCEI). National Ocean and Atmospheric Administration, <https://maps.ngdc.noaa.gov/viewers/bathymetry/>. Accessed July, 2018.
- National Water Information System: Mapper. United States Geological Survey, <https://maps.waterdata.usgs.gov/mapper>. Accessed July, 2018.
- Oki, D. (1999). Geohydrology and numerical simulation of the ground-water flow system of Kona, Island of Hawaii. U.S. Geological Survey, Water-Resources Investigations Report, 99-4073.
- Paerl, H.W. (1997). Coastal eutrophication and harmful algal blooms: Importance of atmospheric deposition and groundwater as “new” nitrogen and other nutrient sources. *Limnology and Oceanography*, 42: 1154-1165.
- Park, S.-C., Yun, S.-T., Chae, G.-T., Yoo, I.-S., Shin, K.-S., Heo, C.-H., and Lee, S.-K. (2005). Regional hydrochemical study on salinization of coastal aquifers, western coastal area of South Korea. *Journal of Hydrology*, 313: 182-194.

- Paytan, A., Shellenbarger, G.G., Street, J.H., Gonnee, M.E., Davis, K., Young, M.B., and Moore, W.S. (2006). Submarine groundwater discharge: An important source of new inorganic nitrogen to coral reef ecosystems. *Limnology and Oceanography*, 51: 343-348.
- Peterson, R.N., Burnett, W.C., Glenn, C.R., and Johnson, A.G. (2009). Quantification of point-source groundwater discharges to the ocean from the shoreline of the Big Island, Hawaii. *Limnology and Oceanography*, 54.3: 890-904.
- Pool, M., Post, V.E.A., and Simmons, C.T. (2015). Effects of tidal fluctuations and spatial heterogeneity on mixing and spreading in spatially heterogeneous coastal aquifers. *Water Resources Research*, 51: 1570-1585.
- Post, V.E.A., Groen, J., Kooi, H., Person, M., Ge, S., and Edmunds W.M. (2013). Offshore fresh groundwater reserves as a global phenomenon. *Nature*, 504: 71-78.
- Remy, N., Boucher, A., and Wu, J. (2009). *Applied Geostatistics with SGeMS*. Cambridge, Cambridge University Press, 263p.
- Robinson, C., Gibbes, B., and Li, L. (2006). Driving mechanisms for groundwater flow and salt transport in a subterranean estuary. *Geophysical Research Letters*, 33.3.
- Ronayne, M.J., Gorelick, S.M., and Zheng, C. (2010). Geological modeling of submeter scale heterogeneity and its influence on tracer transport in a fluvial aquifer. *Water Resources Research*, 46: W10519.
- Ronayne, M.J. and Gorelick, S.M. (2006). Effective permeability of porous media containing branching channel networks. *Physical Review*, 73: 026305.
- Rowland, S.K. and Walker, G.P.L. (1990). Pahoehoe and aa in Hawaii: volumetric flow rate controls the lava structure. *Bulletin of Volcanology*, 52: 615-628.
- Russoniello, C.J., Fernandez, C., Bratton, J.F., Banaszak, F.F., Krantz, D.E., Andres, A.S., Konikow, L.F., and Michael, H.A. (2013). Geologic effects on groundwater salinity and discharge into an estuary. *Journal of Hydrology*, 498: 1-12.
- Sawyer, A.H., David, C.H., Famiglietti, J.S. (2016). Continental patterns of submarine groundwater discharge reveal coastal vulnerabilities. *Science*, 353.6300: 705-707.

- Schlüter, M., Sauter, E.J., Andersen, C.E., Dahlgaard, H., and Dando, P.R. (2004). Spatial distribution and budget for submarine groundwater discharge in Eckernförde Bay (Western Baltic Sea). *Limnology and Oceanography*, 49.1: 157-167.
- Schornberg, C., Schmidt, C., Kalbus, E., and Fleckenstein, J.H. (2010). Simulating the effects of geologic heterogeneity and transient boundary conditions on streambed temperatures – Implications for temperature-based water flux calculations. *Advances in Water Resources*, 33: 1309-1319.
- Sebben, M.L., Werner, A.D., Liggett, J.E., Partington, D., and Simmons, C.T. (2012). On the testing of fully integrated surface-subsurface hydrological models. *Hydrological Processes*, 27.8: 1276-1285.
- Sebben, M.L., Werner, A.D., and Graf, T. (2015). Seawater intrusion in fractured coastal aquifers: A preliminary numerical investigation using a fractured Henry problem. *Advances in Water Resources*, 85: 93-108.
- Sebben, M.L. and Werner, A.D. (2016). On the effects of preferential or barrier flow features on solute plumes in permeable porous media. *Advances in Water Resources*, 98: 32-46.
- Segol, G. and Pinder, G.F. (1976). Transient simulation of saltwater intrusion in southeastern Florida. *Water Resources Research*, 12.1: 65-70.
- Slomp, C.P. and Van Cappellen, P. (2004). Nutrient inputs to the coastal ocean through submarine groundwater discharge: controls and potential impact. *Journal of Hydrology*, 295: 64-86.
- Souza, W.R., and Voss, C.I. (1987). Analysis of an anisotropic coastal aquifer system using variable-density flow and solute transport simulation. *Journal of Hydrology*, 92: 17-41.
- Stieglitz, T., Taniguchi, M., and Neylon, S. (2008). Spatial variability of submarine groundwater discharge, Ubatuba, Brazil. *Estuarine, Coastal, and Shelf Science*, 76: 493-500.
- Street, J.H., Knee, K.L., Grossman, E.E., and Paytan, A. (2008). Submarine groundwater discharge and nutrient addition to the coastal zone and coral reefs of leeward Hawai'i. *Marine Chemistry*, 109: 355-376.
- Sudicky, E.A. and Frind, E.O. (1982). Contaminant transport in fractured porous media: Analytical solutions for a system of parallel fractures. *Water Resources Research*, 18: 1634-1642.

- Tang, D.H., Frind, E.O., and Sudicky, E.A. (1981). Contaminant transport in fracture porous media: Analytical solution for a single fracture. *Water Resources Research*, 17: 555-564.
- Taniguchi, M., Burnett, W.C., Smith, C.F., Paulsen, R.J., O'Rourke, D., Krupa, S.L., and Christoff, J.L. (2003). Spatial and temporal distributions of submarine groundwater discharge rates obtained from various types of seepage meters at a site in the Northeastern Gulf of Mexico. *Biogeochemistry*, 66.1-2: 35-53.
- Uchiyama, Y., Nadaoka, K., Rölke, P., Adachi, K., and Yagi, H. (2000). Submarine groundwater discharge into the sea and associated nutrient transport in a sandy beach. *Water Resources Research*, 36: 1467-1479.
- Webb, E.K. and Anderson, M.P. (1996). Simulation of preferential flow in three-dimensional, heterogeneous conductivity fields with realistic internal architecture. *Water Resources Research*, 32.3: 533-545.
- Wentworth, C.K. and Macdonald, G.A. (1953). Structures and forms of basaltic rocks in Hawaii. *USGS Bulletin* 994.
- Werner, A.D., Bakker, M., Post, V.E.A., Vandenbohede, A., Lu, C., Ataie-Ashtiani, B., Simmons, C.T., and Barry, D.A. (2013). Seawater intrusion processes, investigation, and management: Recent advances and future challenges. *Advances in Water Resources*, 51: 3-26.

Appendix A

TOP-DOWN SALINITY DISTRIBUTIONS FOR EVERY REALIZATION

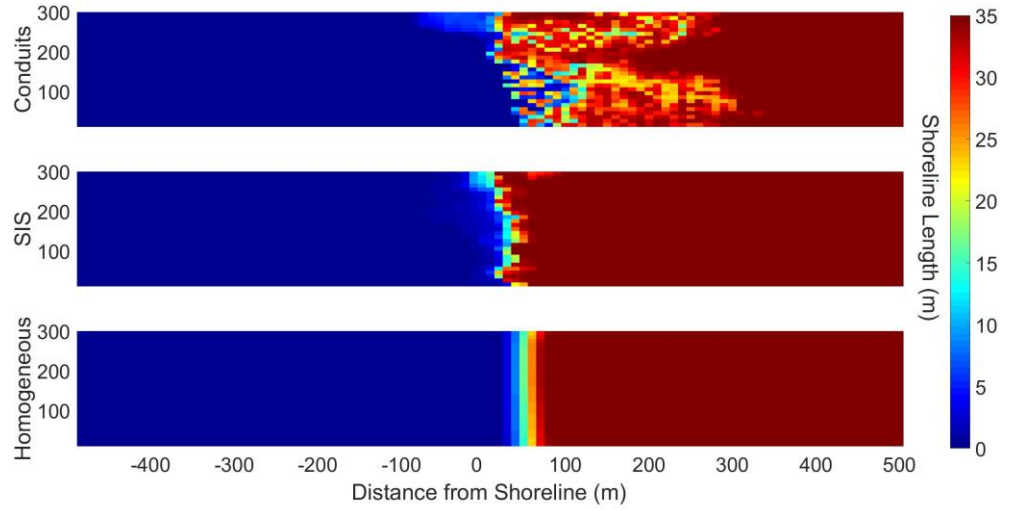


Figure A1. Salinity distributions for Realization 1 (ppt).

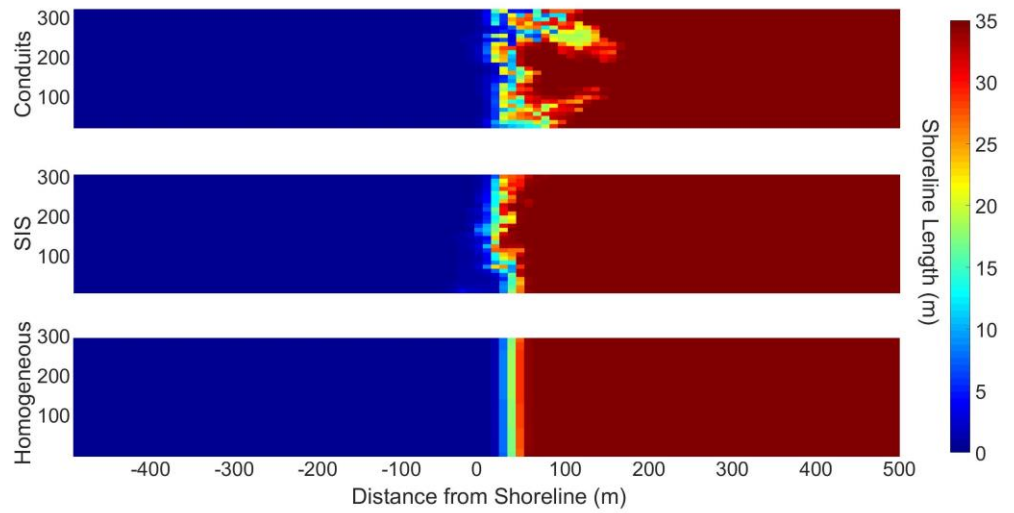


Figure A2. Salinity distributions for Realization 2 (ppt).

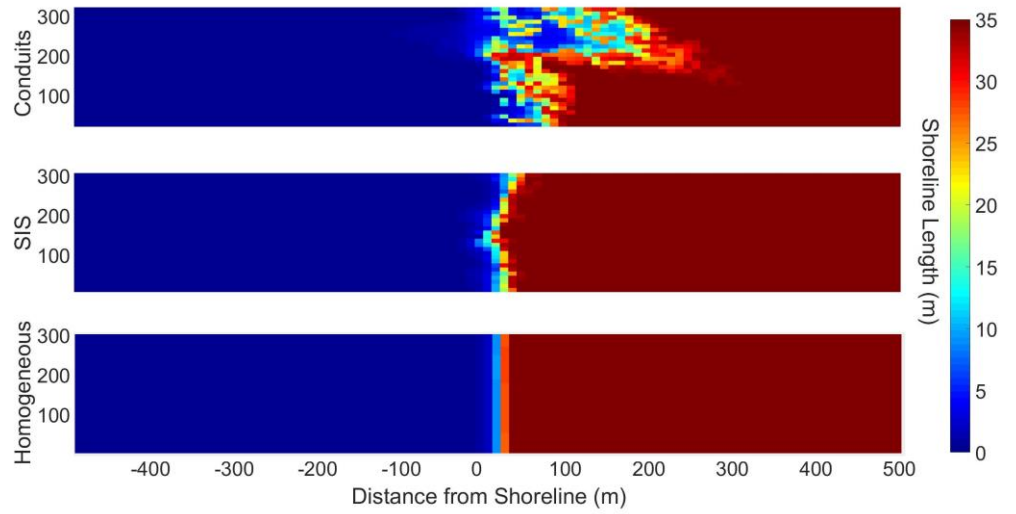


Figure A3. Salinity distributions for Realization 3 (ppt).

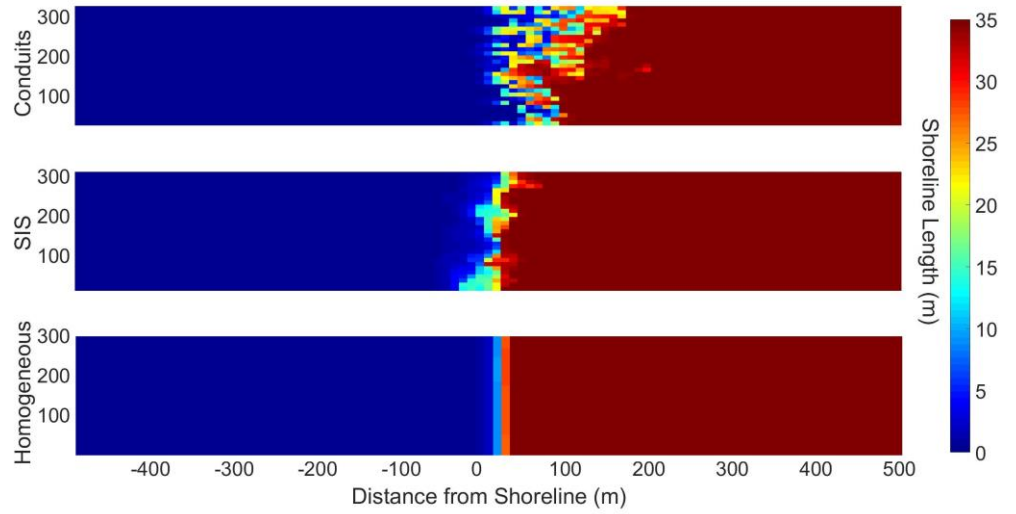


Figure A4. Salinity distributions for Realization 4 (ppt).

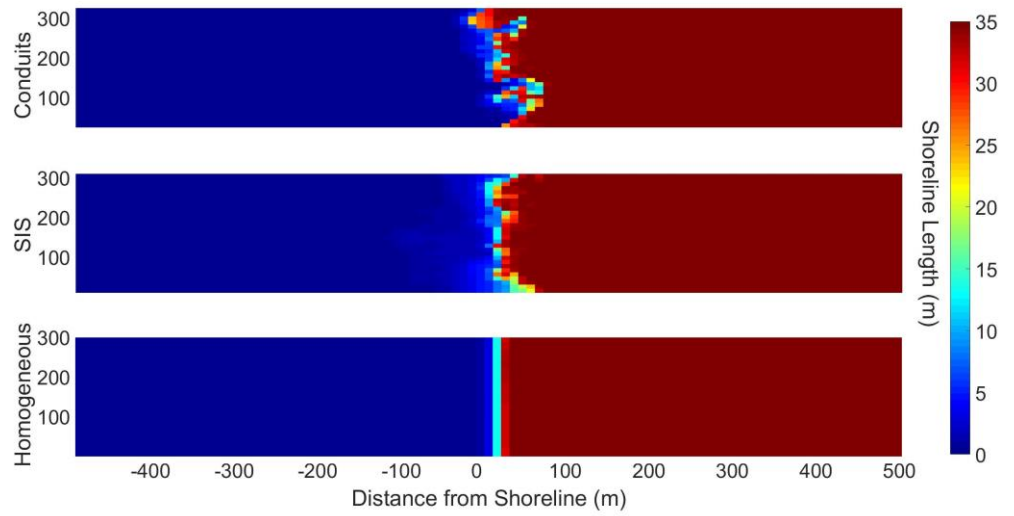


Figure A5. Salinity distributions for Realization 5 (ppt).

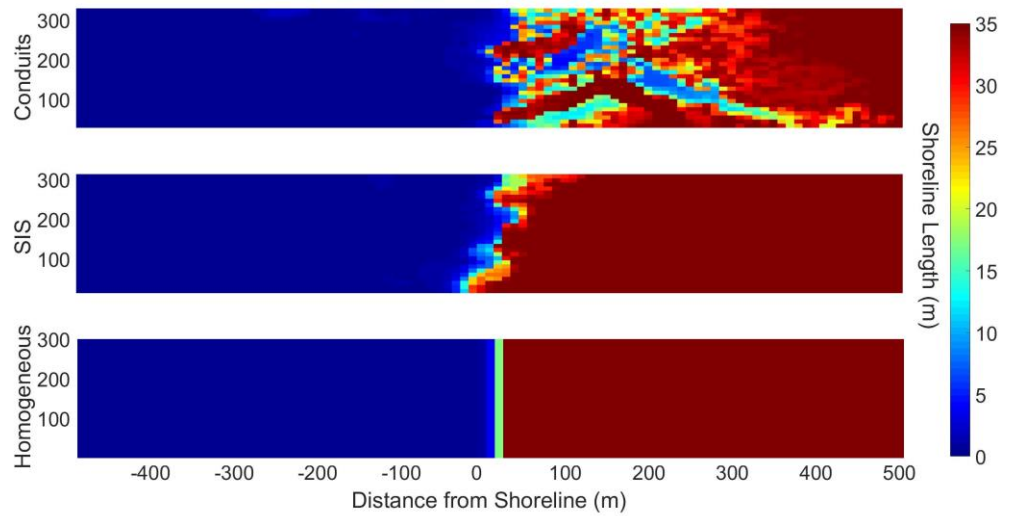


Figure A6. Salinity distributions for Realization 6 (ppt).

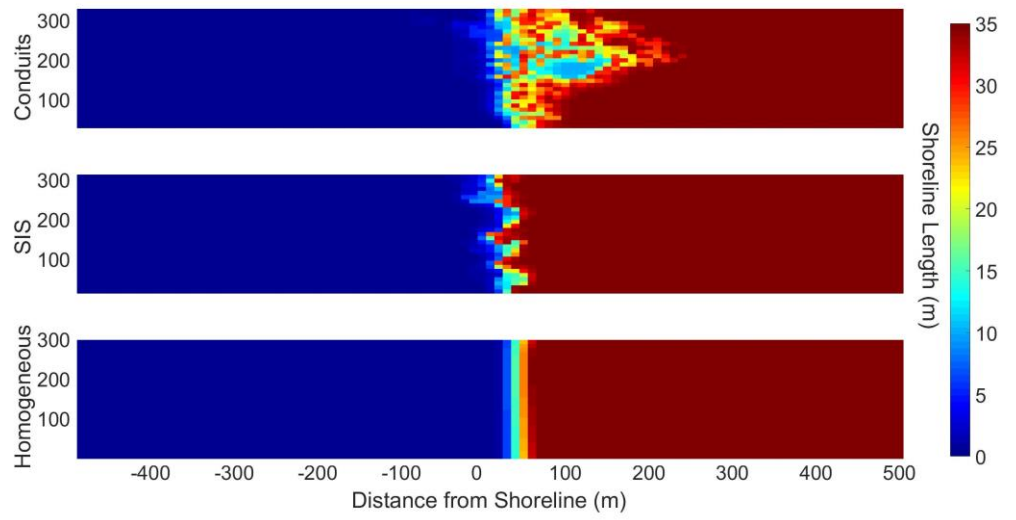


Figure A7. Salinity distributions for Realization 7 (ppt).

Appendix B

TOP-DOWN SGD AND SGR DISTRIBUTIONS FOR EVERY REALIZATION

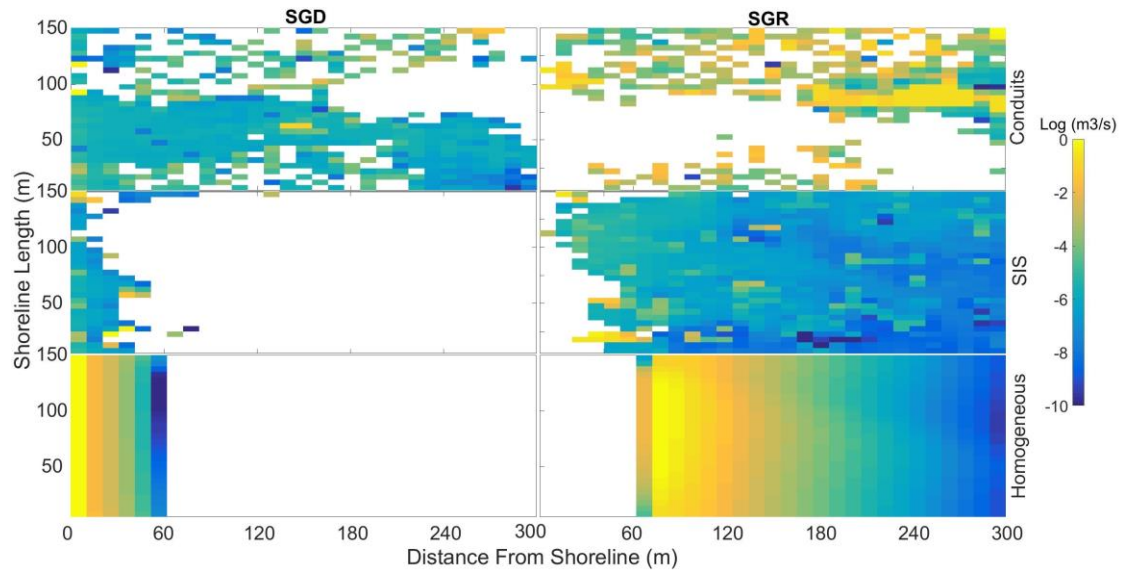


Figure B1. SGD and SGR distributions for Realization 1.

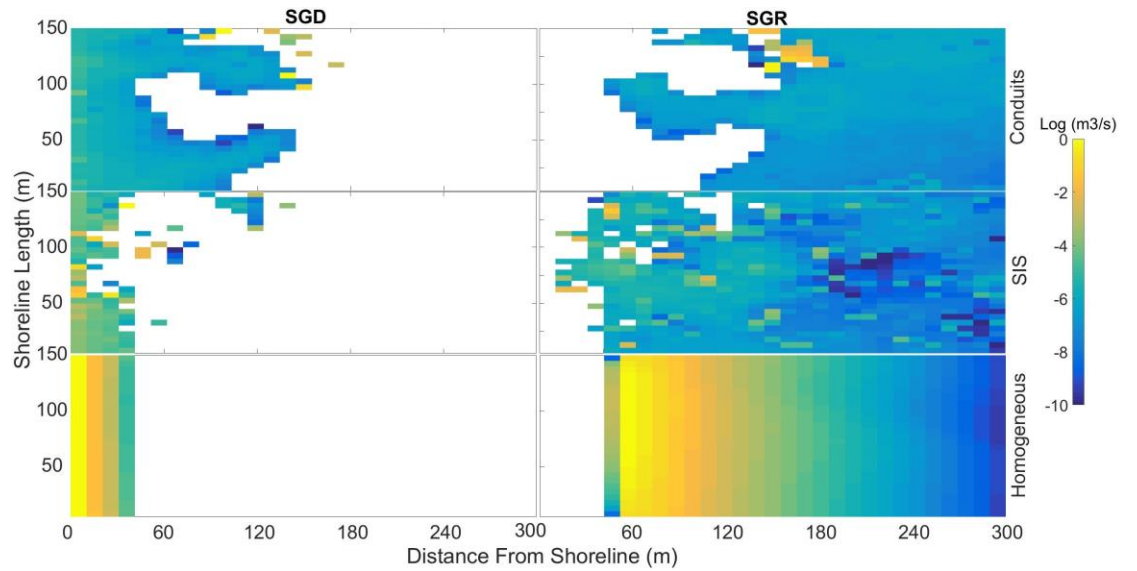


Figure B2. SGD and SGR distributions for Realization 2.

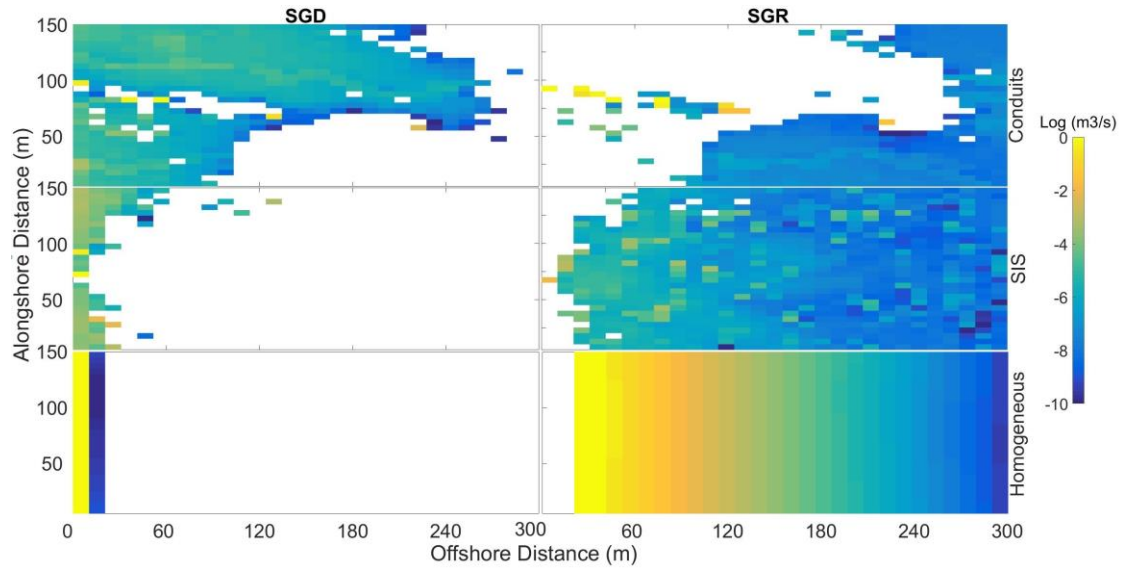


Figure B3. SGD and SGR distributions for Realization 3.

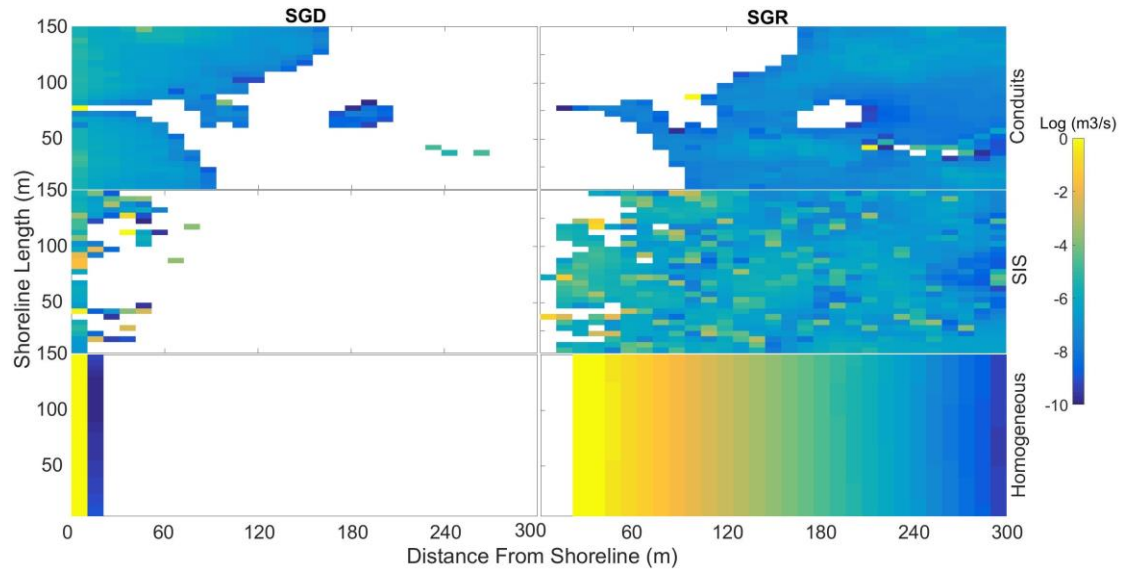


Figure B4. SGD and SGR distributions for Realization 4.

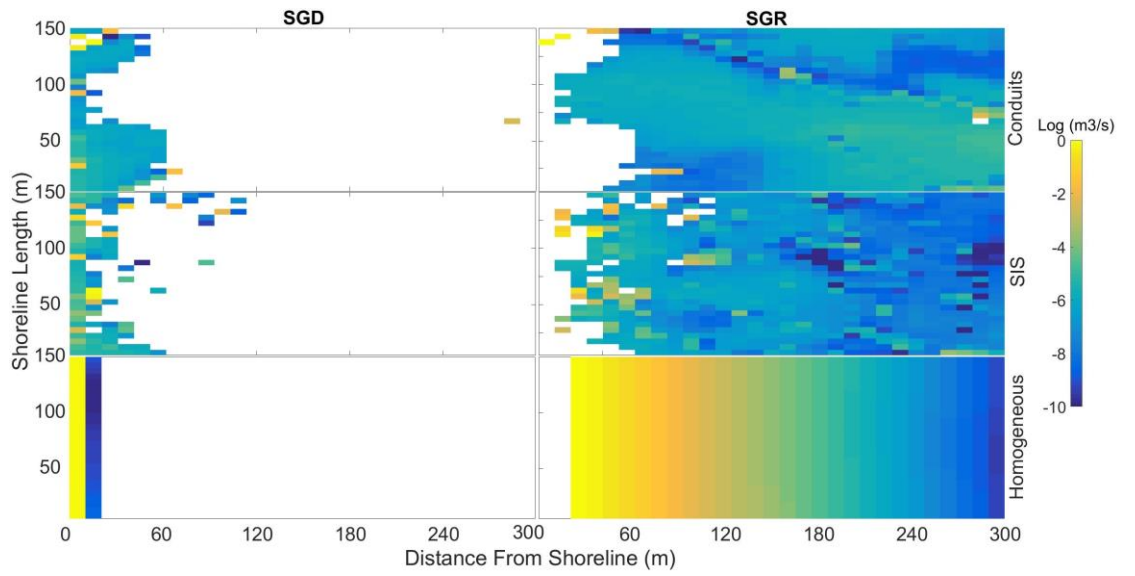


Figure B5. SGD and SGR distributions for Realization 5.

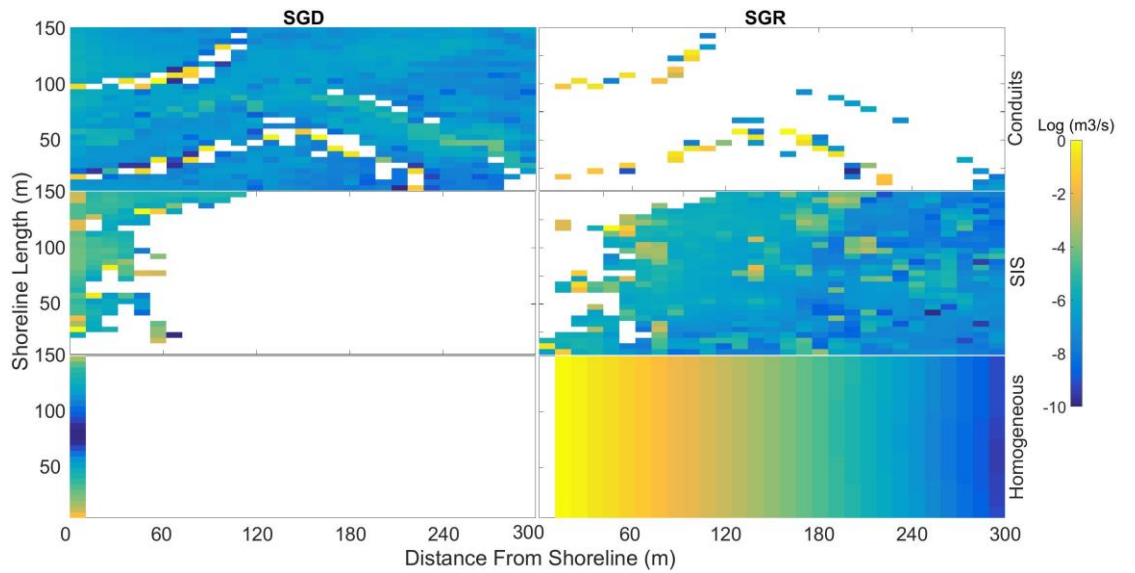


Figure B6. SGD and SGR distributions for Realization 6.

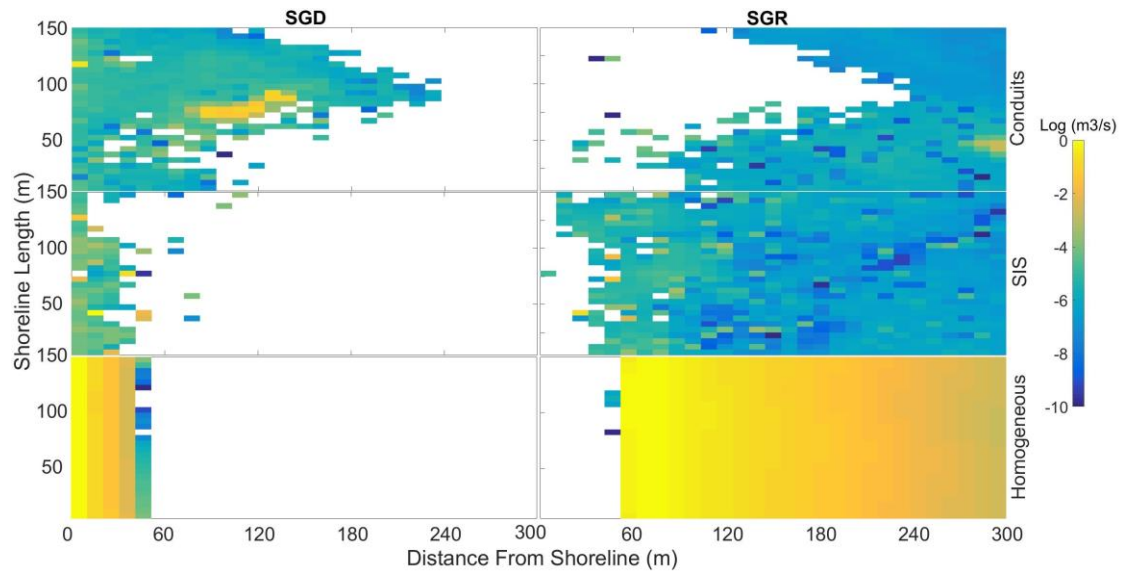


Figure B7. SGD and SGR distributions for Realization 7.

Appendix C

**TABLE OF EFFECTIVE HYDRAULIC CONDUCTIVITIES, RATIOS, AND
LANDWARD SEAWATER EXTENT FOR EACH HOMOGENEOUS
REALIZATION**

Realization #	K_x	K_v	K_x/K_v	Landward Extent of Seawater [m] (Homogeneous)	Landward Extent of Seawater [m] (Conduit)
1	1.42E-04	2.96E-05	4.80	420	170
2	1.33E-05	7.66E-06	1.73	340	140
3	1.59E-05	1.01E-05	1.58	360	250
4	4.67E-06	1.84E-05	0.25	260	240
5	1.31E-04	3.31E-05	3.9	420	170
6	1.17E-04	3.03E-05	3.85	420	450
7	1.07E-04	2.42E-05	4.42	420	160

Appendix D

SALINITY AND HYDRAULIC CONDUCTIVITY CROSS-SECTIONS FOR ALL REALIZATIONS

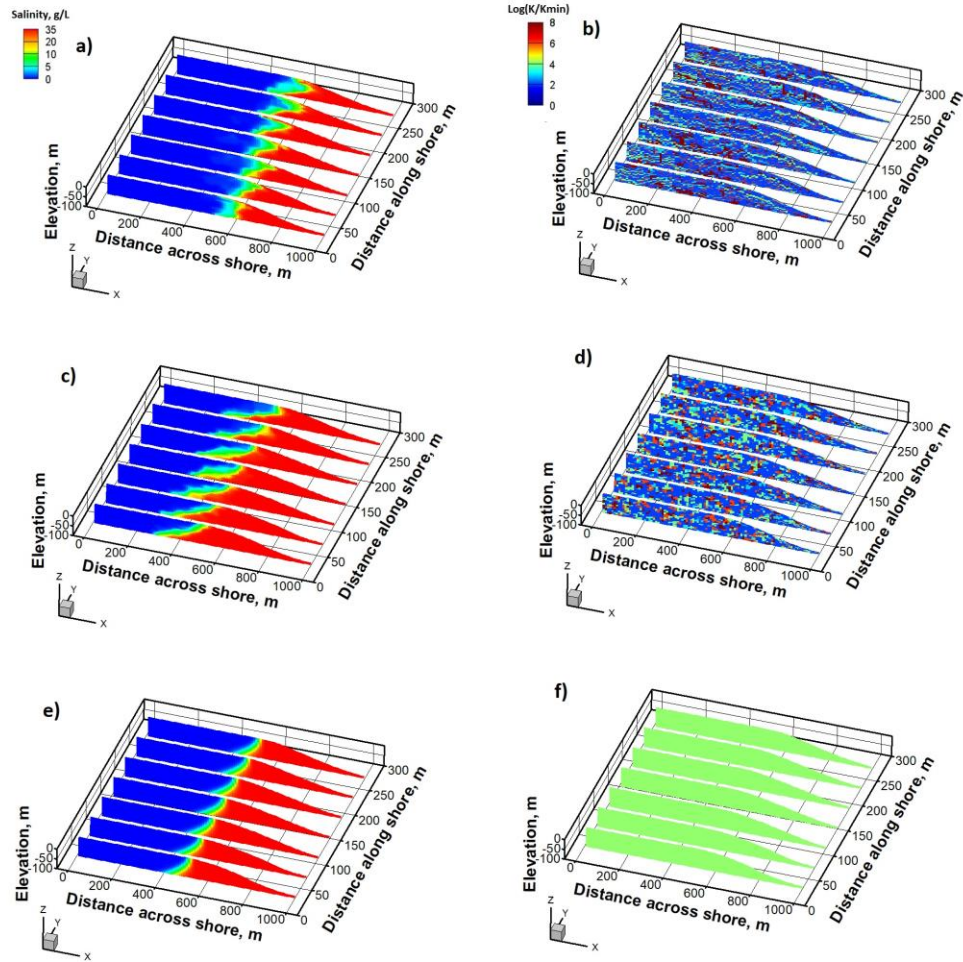


Figure D1. Salinity (left) and hydraulic conductivity (right) cross-sections for conduit (top), SIS (middle), and homogeneous (bottom) cases of Realization 1.

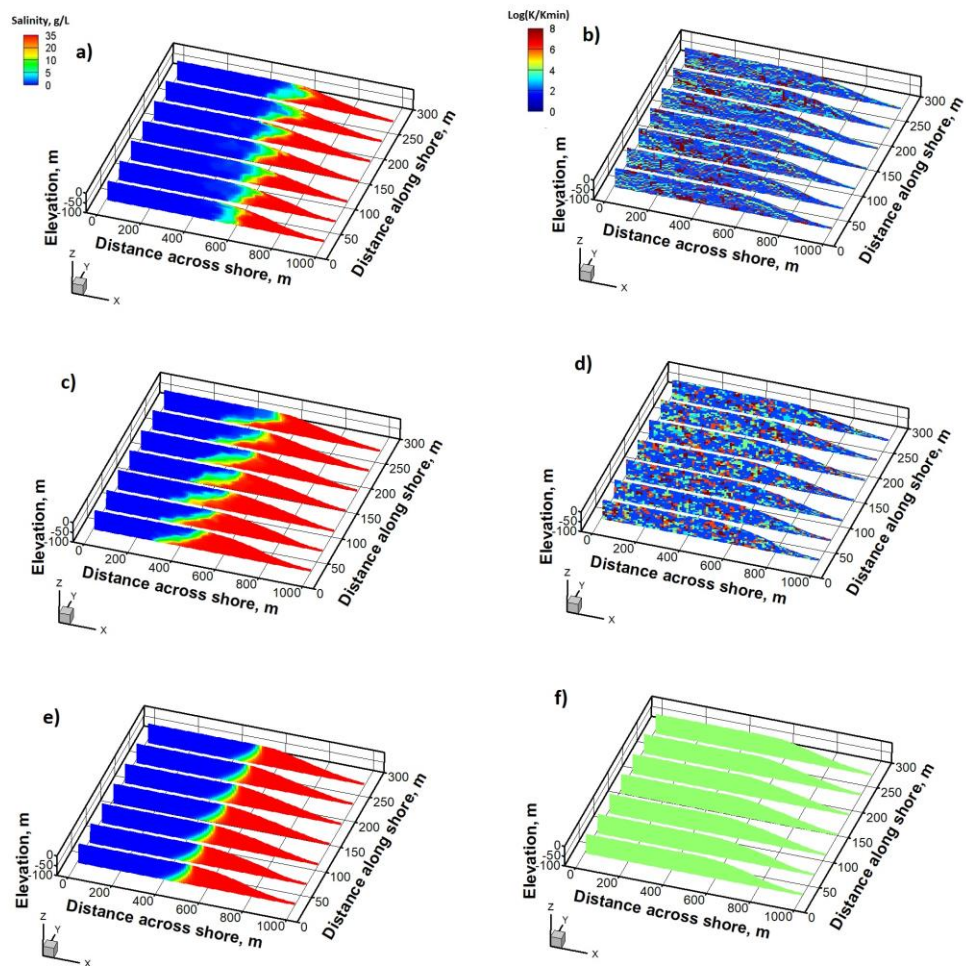


Figure D2. Salinity (left) and hydraulic conductivity (right) cross-sections for conduit (top), SIS (middle), and homogeneous (bottom) cases of Realization 2.

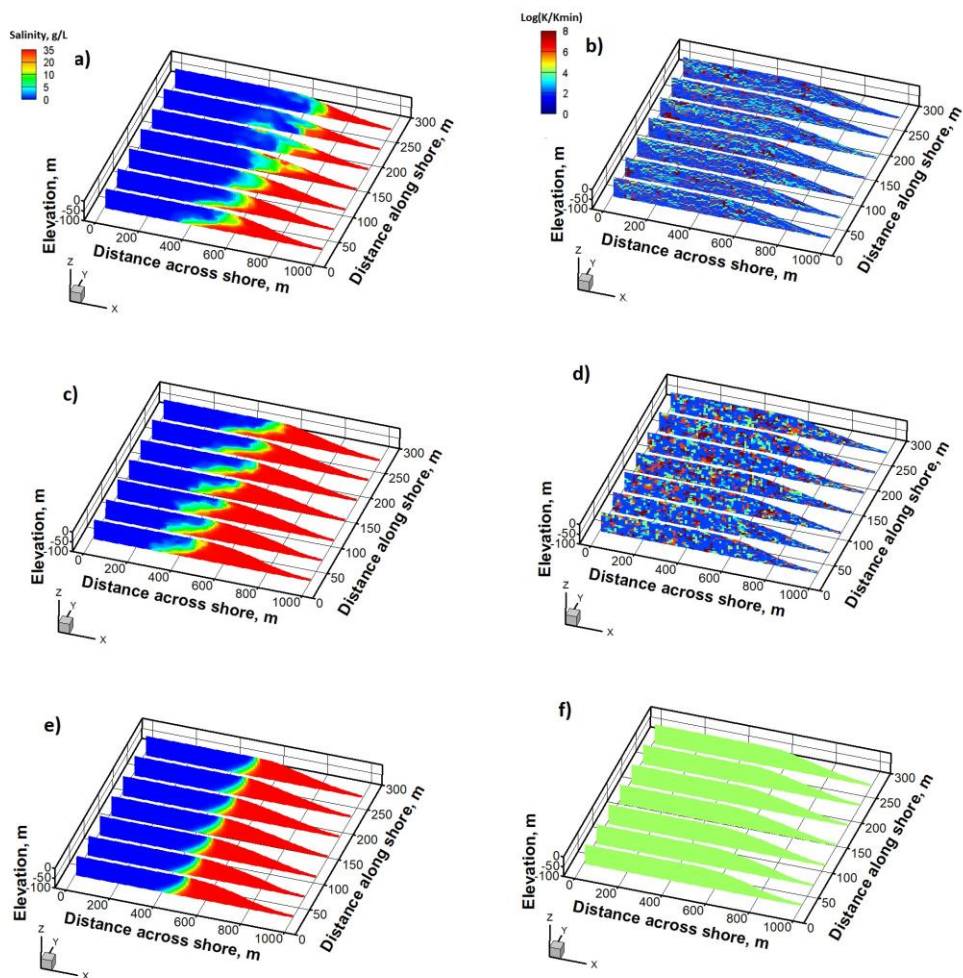


Figure D3. Salinity (left) and hydraulic conductivity (right) cross-sections for conduit (top), SIS (middle), and homogeneous (bottom) cases of Realization 3.

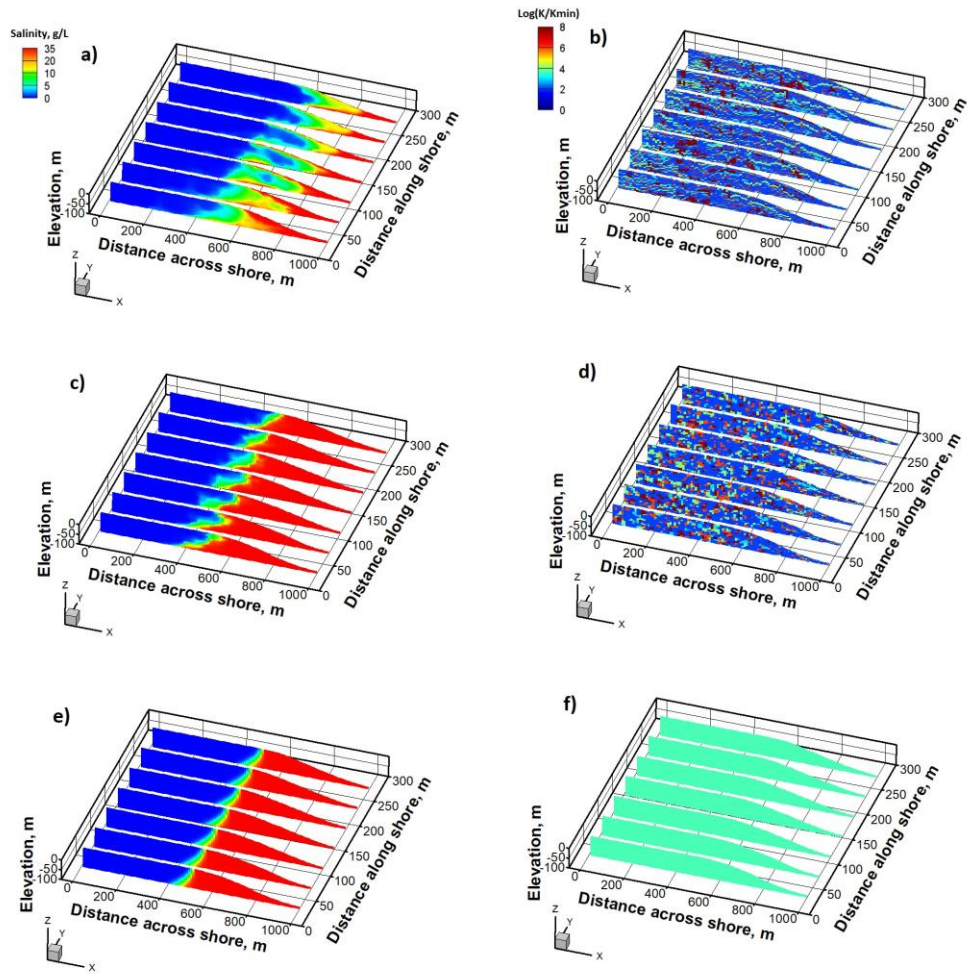


Figure D4. Salinity (left) and hydraulic conductivity (right) cross-sections for conduit (top), SIS (middle), and homogeneous (bottom) cases of Realization 4.

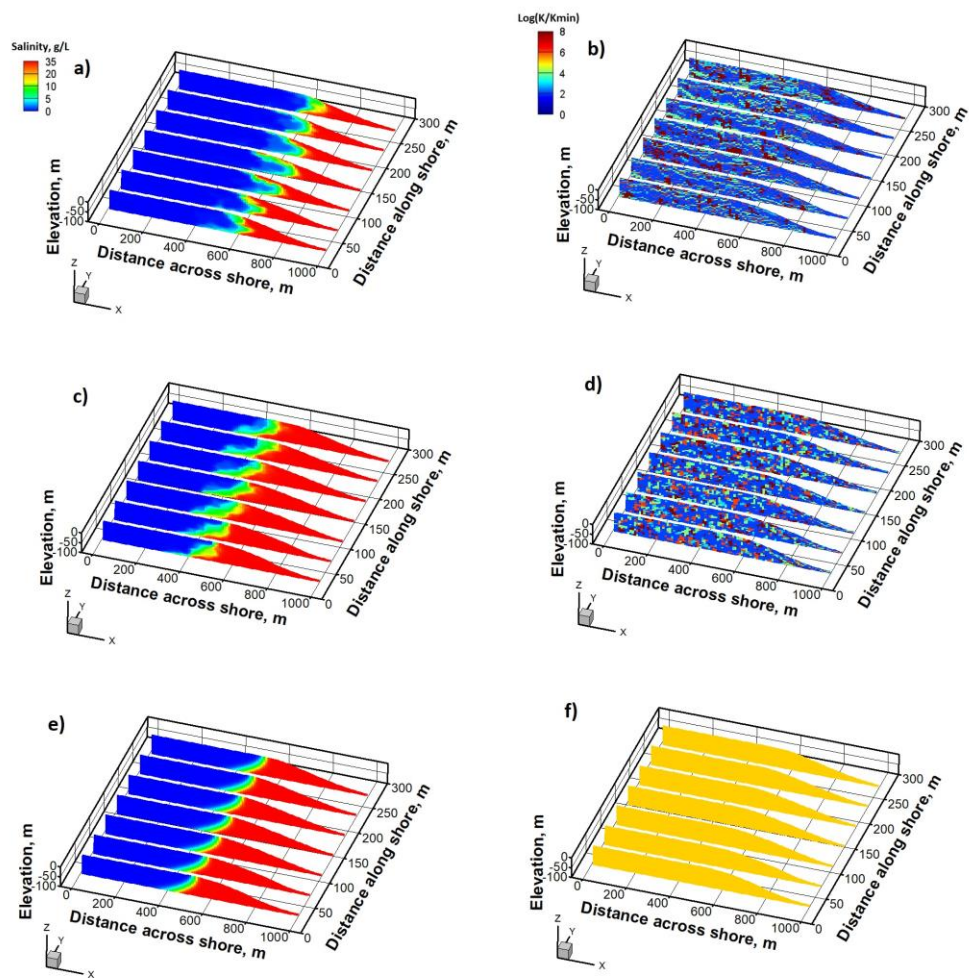


Figure D5. Salinity (left) and hydraulic conductivity (right) cross-sections for conduit (top), SIS (middle), and homogeneous (bottom) cases of Realization 5.

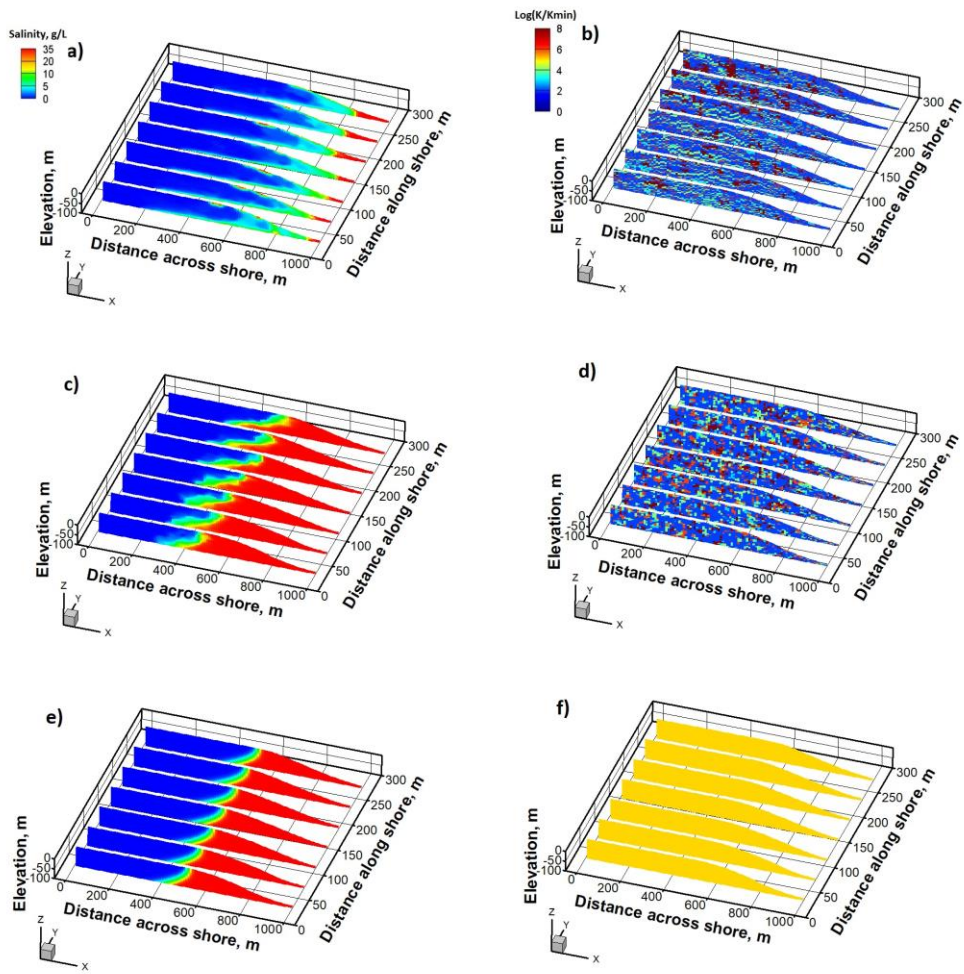


Figure D6. Salinity (left) and hydraulic conductivity (right) cross-sections for conduit (top), SIS (middle), and homogeneous (bottom) cases of Realization 6.

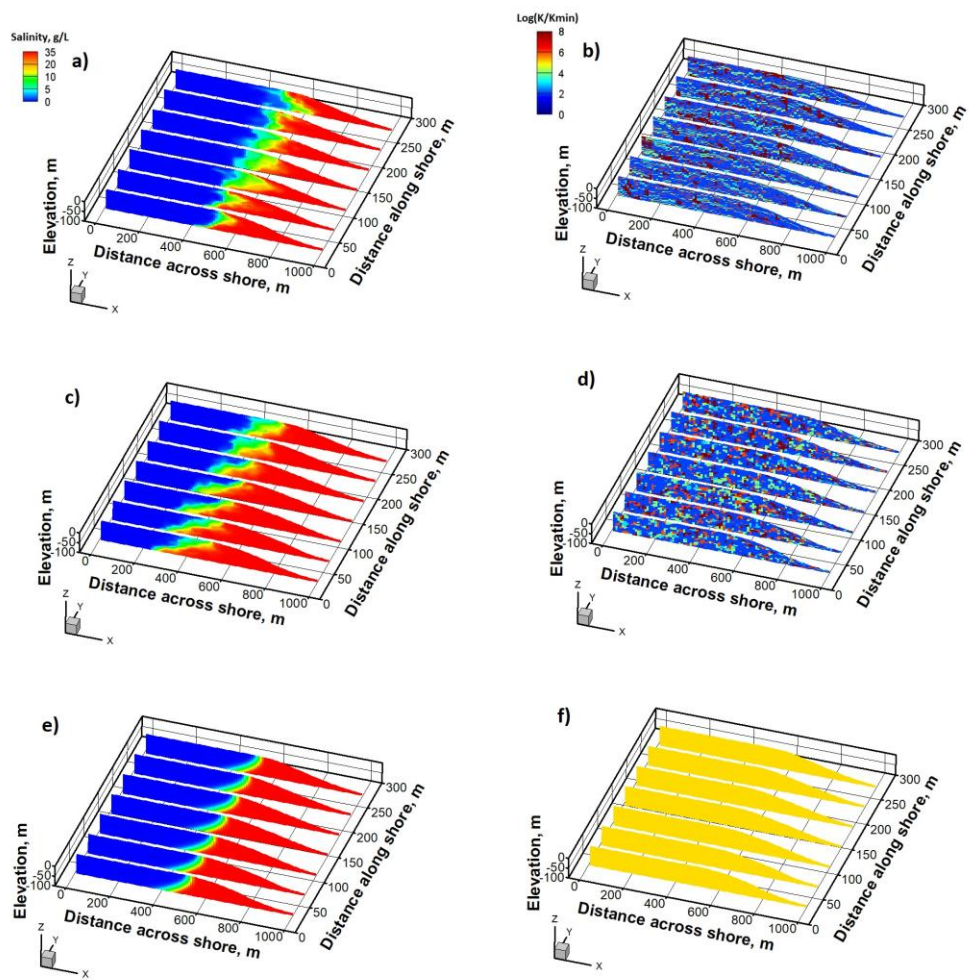


Figure D7. Salinity (left) and hydraulic conductivity (right) cross-sections for conduit (top), SIS (middle), and homogeneous (bottom) cases of Realization 7.